Gauge Invariance in Perturbation Theory

Yongjian Feng

Department of Physics,

McGill University, 3600 University St.

Montreal, P.Q., Canada H3A 2T8

(11 July 1994)

A Thesis submitted to the Faculty of

Graduate Studies and Research

in partial fulfillment of the requirement

for the degree of Master of Science

Name Yongqian Feng

Dissertation Abstracts International is arranged by broad, general subject categories. Please select the one subject which most nearly describes the content of your dissertation. Enter the corresponding four-digit code in the spaces provided.

High energy and elementary particles | 0798

SUBJECT TERM | SUBJECT CODE

U·M·I

Subject Categories

THE HUMANITIES AND SOCIAL SCIENCES

COMMUNICATIONS AND THE ARTS

Architecture	0729
Art History	0377
Cinema	0900
Dance	0378
Fine Arts	0357
Information Science	0723
Journalism	0391
Library Science	0399
Mass Communications	0708
Music	0413
Speech Communication	0459
Theater	0465

EDUCATION

General	0515
Administration	0514
Adult and Continuing	0516
Agricultural	0517
Art	0273
Bilingual and Multicultural	0282
Business	0688
Community College	0275
Curriculum and Instruction	0727
Early Childhood	0518
Elementary	0524
Finance	0277
Guidance and Counseling	0519
Health	0680
Higher	0745
History of	0520
Home Economics	0278
Industrial	0521
Language and Literature	0279
Mathematics	0280
Music	0522
Philosophy of	0998
Physical	0523
Psychology	0525
Reading	0535
Religious	0527
Sciences	0714
Secondary	0533
Social Sciences	0534
Sociology of	0340
Special	0529
Teacher Training	0530
Technology	0710
Tests and Measurements	0288
Vocational	0747

LANGUAGE, LITERATURE AND LINGUISTICS

Language	
General	0679
Ancient	0289
Linguistics	0290
Modern	0291
Literature	
General	0401
Classical	0294
Comparative	0295
Medieval	0297
Modern	0298
African	0316
American	0591
Asian	0305
Canadian (English)	0352
Canadian (French)	0355
English	0593
Germanic	0311
Latin American	0312
Middle Eastern	0315
Romance	0313
Slavic and East European	0314

PHILOSOPHY, RELIGION AND THEOLOGY

Philosophy	0422
Religion	
General	0318
Biblical Studies	0321
Clergy	0319
History of	0320
Philosophy of	0322
Theology	0469

SOCIAL SCIENCES

American Studies	0323
Anthropology	
Archaeology	0324
Cultural	0326
Physical	0327
Business Administration	
General	0310
Accounting	0272
Banking	0770
Management	0454
Marketing	0338
Canadian Studies	0385
Economics	
General	0501
Agricultural	0503
Commerce-Business	0505
Finance	0508
History	0509
Labor	0510
Theory	0511
Folklore	0358
Geography	0366
Gerontology	0351
History	
General	0578
Ancient	0579
Medieval	0581
Modern	0582
Black	0328
African	0331
Asia, Australia and Oceania	0332
Canadian	0334
European	0335
Latin American	0336
Middle Eastern	0333
United States	0337
History of Science	0585
Law	0398
Political Science	
General	0615
International Law and Relations	0616
Public Administration	0617
Recreation	0814
Social Work	0452
Sociology	
General	0626
Criminology and Penology	0627
Demography	0938
Ethnic and Racial Studies	0631
Individual and Family Studies	0628
Industrial and Labor Relations	0629
Public and Social Welfare	0630
Social Structure and Development	0700
Theory and Methods	0344
Transportation	0709
Urban and Regional Planning	0999
Women's Studies	0453

THE SCIENCES AND ENGINEERING

BIOLOGICAL SCIENCES

Agriculture	
General	0473
Agronomy	0285
Animal Culture and Nutrition	0475
Animal Pathology	0476
Food Science and Technology	0359
Forestry and Wildlife	0478
Plant Culture	0479
Plant Pathology	0480
Plant Physiology	0817
Range Management	0777
Wood Technology	0746
Biology	
General	0306
Anatomy	0287
Biostatistics	0308
Botany	0309
Cell	0379
Ecology	0329
Entomology	0353
Genetics	0369
Limnology	0793
Microbiology	0410
Molecular	0307
Neuroscience	0317
Oceanography	0416
Physiology	0433
Radiation	0821
Veterinary Science	0778
Zoology	0472
Biophysics	
General	0786
Medical	0760

EARTH SCIENCES

Biogeochemistry	0425
Geochemistry	0996
Geodesy	0370
Geology	0372
Geophysics	0373
Hydrology	0388
Mineralogy	0411
Paleobotany	0345
Paleoecology	0426
Paleontology	0418
Paleozoology	0985
Palynology	0427
Physical Geography	0368
Physical Oceanography	0415

HEALTH AND ENVIRONMENTAL SCIENCES

Environmental Sciences	0768
Health Sciences	
General	0566
Audiology	0300
Chemotherapy	0992
Dentistry	0567
Education	0350
Hospital Management	0769
Human Development	0758
Immunology	0982
Medicine and Surgery	0564
Mental Health	0347
Nursing	0569
Nutrition	0570
Obstetrics and Gynecology	0380
Occupational Health and Therapy	0354
Ophthalmology	0381
Pathology	0571
Pharmacology	0419
Pharmacy	0572
Physical Therapy	0382
Public Health	0573
Radiology	0574
Recreation	0575
Speech Pathology	0460
Toxicology	0383
Home Economics	0386

PHYSICAL SCIENCES

Pure Sciences

Chemistry	
General	0485
Agricultural	0749
Analytical	0486
Biochemistry	0487
Inorganic	0488
Nuclear	0738
Organic	0490
Pharmaceutical	0491
Physical	0494
Polymer	0495
Radiation	0754
Mathematics	0405
Physics	
General	0605
Acoustics	0986
Astronomy and Astrophysics	0606
Atmospheric Science	0608
Atomic	0748
Electronics and Electricity	0607
Elementary Particles and High Energy	0798
Fluid and Plasma	0759
Molecular	0609
Nuclear	0610
Optics	0752
Radiation	0756
Solid State	0611
Statistics	0463

Applied Sciences

Applied Mechanics	0346
Computer Science	0984
Engineering	
General	0537
Aerospace	0538
Agricultural	0539
Automotive	0540
Biomedical	0541
Chemical	0542
Civil	0543
Electronics and Electrical	0544
Heat and Thermodynamics	0348
Hydraulic	0545
Industrial	0546
Marine	0547
Materials Science	0794
Mechanical	0548
Metallurgy	0743
Mining	0551
Nuclear	0552
Packaging	0549
Petroleum	0765
Sanitary and Municipal	0554
System Science	0790
Geotechnology	0428
Operations Research	0796
Plastics Technology	0795
Textile Technology	0994

PSYCHOLOGY

General	0621
Behavioral	0384
Clinical	0622
Developmental	0620
Experimental	0623
Industrial	0624
Personality	0625
Physiological	0989
Psychobiology	0349
Psychometrics	0632
Social	0451

Abstract

Gauge theories and their BRST invariance are reviewed. Gauge-invariant (color) subamplitudes for non-Abelian gauge theories are discussed. BRST transformations of non-Abelian vertices are derived, and are used to obtain the gauge transformation of any Feynman diagram. From this minimal sets of gauge-invariant subamplitudes in perturbation theory can be found. This knowledge is useful in the application of the spinor helicity technique, and is indispensible for future developments of non-Abelian perturbation theories.

RÉSUMÉ

Les théories des jauges et leur invariance BRST sont passées en revue dans cette thèse. Les sous-amplitudes invariantes de jauge (de couleur) associées aux théories des jauges non-abéliennes y sont discutées. Les transformations BRST de sommets non-abéliens sont dérivées et utilisées pour obtenir la transformation de jauge de tout diagramme de Feynman. Des ensembles minimaux de sous-amplitudes invariantes de jauge obtenues par la théorie des perturbations peuvent alors être trouvés. Ce résultat est utile à l'application de la technique de l'hélicité spinorielle et indispensable au développement futur des théories des perturbations non-abéliennes.

List of Figures

Contents

I. INTRODUCTION

The central theme of this thesis is to study the gauge variation of Feynman diagrams. This Introduction serves to explain this problem and why it is important.

The present theory of elementary particle physics is the Standard Model. It explains every available experiment in strong, electromagnetic, and weak interactions, provided the measured quantities can be calculated by the perturbation theory. The Standard Model is given by a $G = SU(3)_{color} \times SU(2)_L \times U(1)_Y$ gauge theory, so to understand in general its implications and in particular why we are interested in the certain problem discussed in this thesis , we must first have some feeling as to what a gauge theory is.

The first and standard example of a gauge theory is the Maxwell theory of electrodynamics. What is so special about this theory is that although the photon has spin 1, only two circularly polarized states of the photon are present instead of the three normally associated with a spin-1 particle. This fact is intimately related to the masslessness of the photon, for in this theory, the absence of a photon mass is actually ensured by the presence of only two photon polarizations (a massive spin-1 particle must have three polarizations). A gauge theory is roughly speaking such a theory, that the number of polarizations present for a spin-1 particle is two rather than three.

Mathematically, the photon in the Maxwell theory is described by a vector potential $A_\mu(x)$, introduced in such a way that the physics is completely unaltered if an arbitrary gradient is added to this field, *i.e.*, if $A_\mu(x)$ is replaced by $A_\mu(x) + \partial_\mu\lambda(x)$ for an arbitrary $\lambda(x)$. This change is known as a *gauge transformation* and the physical invariance is called a *gauge invariance.* This invariance ensures that the longitudinal component of $A_\mu(x)$ is physically meaningless (because it can be arbitrary), thus it must be decoupled, and hence gauge arbitraries greatly complicate the formalism, especially in a quantum theory where only physical degrees of freedom should be quantized. The asymmetry thus introduced between the different components makes life difficult. Nevertheless, by using the Feynman path integral technique, this difficulty can be largely overcome, because in this formalism symmetry is somewhat restored in that even the unphysical longitudinal degree of freedom can be quantized, but at the expense of having to introduce an extra unphysical degree of freedom called the *ghost* to compensate for the longitudinal contribution and to decouple it.

An important property of the Maxwell theory is that the photon couples universally to the electric charge. The coupling between a photon and a charge particle depends on the charge of the particle but not whether it is a proton or a positron. This particular property of the theory actually follows from the gauge invariance discussed above.

In 1954, Yang and Mills [1] were able to generalize the Maxwell theory into a new kind of gauge theories possessing most of these special attributes . However, there are now more than one 'photon', or more correctly, the analogy of the photons in this theory called the *gauge particles.* The gauge particles in this 'non-Abelian' gauge theory are still coupled universally, but instead to the electric charge of particles as in the Maxwell theory, they are now coupled to some 'non-Abelian charges'. A 'non-Abelian charge' is a quantum number that does not add arithmetically. Isotopic spin is a typical example, for although its third component adds arithmetically, because of the uncertainly principle the other two components do not. It turns out that whatever the non-Abelian charge is, the gauge particles themselves must also carry such a charge and hence they must couple to themselves as well. This is different from the photons of the Maxwell theory which are neutral and do not directly couple among themselves. For that reason, the Yang-Mills theory turns out to be a more complicated gauge theory.

According to the Noether theorem, a conserved charge is associated with a symmetry group of the dynamics. For example, the conserved electric charge in the Maxwell theory is associated with a $U(1)_{em}$ invariance. In general, an arithmetically additive quantum number is associated with a $U(1)$ group, and a non-Abelian charge is associated with a non-Abelian (non-commutative) group like $SU(N)$. Every hadron carries a non-Abelian charge called *color*, associated with the symmetry group $SU(3)_{color}$, and according to the Standard Model it is this color that is the source of all strong interactions. Similarly, every particle carries a *weak isospin* associated with the group $SU(2)_L$, and a *weak hypercharge* associated with the group $U(1)_Y$, and it is the universal coupling to these charges that is responsible for the electromagnetic and the weak interactions.

Quantum field theories are difficult theories to compute, and most of the known results are obtained in perturbation theories. Perturbation-theory calculations proceed through the evaluation of *Feynman diagrams.* For a complicated process, and when a high degree of accuracy is required, many diagrams have to be evaluated with each diagram containing many terms This is especially bad for gauge theories, for each Feynman diagram is generally not gauge invariant, though the sum, representing a physical process, must be. In other words, many gauge-dependent terms must be present in individual diagrams that eventually get cancelled out. In non-Abelian gauge theories where there are more diagrams and more terms than the Maxwell theory, the complication can become so serious as to retard seriously our ability for computations. For that reason it is important to find ways to calculate these diagrams that the gauge-dependent terms, which eventually must be cancelled out at the end, occur as little as possible in individual diagrams. Under a gauge transformation, the content of different diagrams mix, so it is conceivable that a suitable gauge choice can result in having less gauge-dependent terms in each diagram. In fact, a special technique known as the *spinor helicity technique* [2] [3] is available to help us simplify matters along these lines. Recently it was also realized that reorganization in a superstring-like way can accomplish some of the goals as well [4] [5]. To be able to devise new techniques along these lines, or even to be able to utilize the existing techniques efficiently, we must understand thoroughly how a gauge transformation shifts the contents of a Feynman diagram to another. The study of this problem is the central theme of this thesis. For this purpose, this thesis is arranged as follows: In Sec.II, we briefly review the contents of Abelian and non-Abelian gauge theories. Then we use current conservation to discuss the so-called Ward-Takahashi identity in QED in Sec.III. A review of BRST transformation is presented in Sec.IV, together with an application of this transformation in proving Ward-Takahashi identity and Slavnov-Taylor identity. Finally, in Sec.V, we use BRST invariance to discuss the gauge invariance of perturbative scattering amplitudes in QED, and in QCD, especially the gauge invariant subsets in both of them.

II. GAUGE THEORIES: QED AND QCD

In this thesis, we will use the following metric

$$g = \begin{pmatrix} 1 & 0 & 0 & 0 \\ 0 & -1 & 0 & 0 \\ 0 & 0 & -1 & 0 \\ 0 & 0 & 0 & -1 \end{pmatrix}$$

A. Abelian gauge theory: QED

The QED Lagrangian is

$$\mathcal{L} = \bar{\psi} i\gamma^{\mu}(\partial_{\mu} + ieA_{\mu})\psi - m\bar{\psi}\psi - \frac{1}{4}F_{\mu\nu}F^{\mu\nu} \ , \tag{2.1}$$

where

$$F^{\mu\nu} = \partial^{\mu}A^{\nu} - \partial^{\nu}A^{\mu} \ . \tag{2.2}$$

$\psi(x)$ is the spinor field satisfying the following equal-time anti-commutation relation

$$\delta(x^0 - y^0)[\psi(x), \psi^{\dagger}(y)]_{+} = \delta^4(x - y) \ , \tag{2.3}$$

and $A(x)$ is the vector potential for the photon field.

The local symmetry for QED is a $U(1)$ gauge symmetry. The corresponding local transformations are

$$\begin{aligned} \psi(x) &\rightarrow \psi(x)' = e^{-i\alpha(x)}\psi(x) \ , \\ \bar{\psi}(x) &\rightarrow \bar{\psi}(x)' = e^{i\alpha(x)}\bar{\psi}(x) \ , \\ A_{\mu}(x) &\rightarrow A'_{\mu}(x) = A_{\mu}(x) + \frac{1}{e}\partial_{\mu}\alpha(x) \ , \end{aligned} \tag{2.4}$$

where $\alpha(x)$ is the local infinitesimal transformation parameter. The Lagrangian is invariant under this transformation, as is the action S, which is defined to be the space-time integral of the Lagrangian density.

To determine the conserved current, we must use *Noether's theorem*, which states that for each continuous symmetry that preserves the action

$$S = \int L dt \ , \tag{2.5}$$

there is a conserved current J satisfying

$$\partial_\mu J^\mu = 0 \ . \tag{2.6}$$

The corresponding charge Q given by

$$Q = \int d^3x J_0(x) \tag{2.7}$$

is a constant of the motion. Note we used L as the Lagrangian and $\mathcal{L}$ as the Lagrangian density:

$$L = \int d^3x \mathcal{L} \ . \tag{2.8}$$

The proof of Noether's theorem can be found in any text book [6] [7].

For QED, its conserved current is related to its $U(1)$ global symmetry, and is given by

$$J_\mu = \bar{\psi}\gamma_\mu\psi \ . \tag{2.9}$$

The charge is just the electric charge Q

$$\begin{aligned} Q(t) &= \int d^3x J_0(x) \\ &= \int d^3x (\psi^\dagger(x)\psi(x)) \ . \end{aligned} \tag{2.10}$$

B. Non-Abelian gauge theory: QCD

QCD is more difficult than QED because the local transformation is now a *non-Abelian* $SU(3)$ color group, which has many generators that do not all commute with one another.

The non-Abelian gauge theory was first studied by Yang and Mills in 1954. They tried to use it to describe the interactions between hadrons which possess an $SU(2)$ isotopic spin symmetry. We know now that $SU(2)$ is only an approximate symmetry in strong interactions, but their formalism can be equally well applied to the $SU(3)$ color symmetry which is believed to hold in *strong* interactions between the constituents of the hadrons.

We shall now discuss the non-Abelian gauge theory possessing an $SU(N)$ symmetry. The group $SU(N)$ has $N^2 - 1$ generators. We shall use the following symbols,

$$T^a \ (a = 1, \cdots, N^2 - 1) \ , \tag{2.11}$$

to denote the generator matrices in the fundamental representation, normalized such that

$$tr(T^a T^b) = \delta^{ab} \ . \tag{2.12}$$

The commutation relation defining the structure of the group is given by

$$[T^a, T^b] = i f^{abc} T^c \ , \tag{2.13}$$

where the structure constant f^{abc} can be taken to be totally antisymmetric in its indices on account of (2.12) and (2.13).

The infinitesimal gauge transformation of fermion field $\Psi(x)$ in the fundamental representation is

$$\delta\Psi(x) \to -iT \cdot \alpha(x)\Psi(x) \ , \tag{2.14}$$

where $T \cdot \alpha(x) = T^a \alpha^a(x)$. To compensate for the local variation of (2.14), we must introduce the (gauge) fields $A_\mu(x) = A_\mu^a(x) T^a$, which transforms like

$$\delta A_\mu^a = -\frac{1}{g}\partial_\mu \alpha^a + f^{abc} A_\mu^c \alpha^b \ , \tag{2.15}$$

where g is the coupling constant, the analogy of the e in QED, and the covariant derivative

$$D^\mu = \partial^\mu - igA^\mu(x) \tag{2.16}$$

into the Lagrangian, as in QED. Accordingly, the gauge-invariant Lagrangian can be obtained from the free-field Lagrangian by replacing the derivative ∂ with the covariant derivative D:

$$\mathcal{L} = \bar{\Psi}(x)(i\gamma_\mu D^\mu - m)\Psi(x) - \frac{1}{4}tr(F_{\mu\nu}F^{\mu\nu}) , \tag{2.17}$$

where $F_{\mu\nu} = F^a_{\mu\nu}T^a$ and

$$F^a_{\mu\nu} \equiv \partial_\mu A^a_\nu - \partial_\nu A^a_\mu + gf^{abc}A^b_\mu A^c_\nu . \tag{2.18}$$

Path integral is the most convenient tool to quantize a gauge theory. In its most straightforward form, the vacuum functional is given by the path integral of the exponential of the action:

$$W \sim \int [dA_\mu] \exp\left(i\int d^4x\mathcal{L}(x)\right) . \tag{2.19}$$

However, this path integral is not well-defined because gauge invariance makes it infinite. To see that, imagine the integration space to be made up of a series of hypersurfaces, obtained from one another by gauge transformations. If we divide the path integration in (2.19) first into integrations on these hypersurfaces, and then integrations perpendicular to these hypersurfaces, then the latter integral is divergent because gauge invariance of the action $S = \int d^4x\mathcal{L}(x)$. For that reason the sensible path integral should be carried out over only one of these many hypersurfaces.

There are no unique way to determine these hypersurfaces. Suppose the hypersurface on which to carry out the path integral is defined by the gauge-fixing condition

$$f^a(A_\mu) = 0 , \tag{2.20}$$

then the naive vacuum functional is given by

$$W \sim \int [dA_\mu] \frac{1}{\Delta_f} [d\theta] \delta(f^a(A_\mu^\theta)) \exp\left(i \int d^4x \mathcal{L}(x)\right) , \tag{2.21}$$

where we have inserted

$$\frac{1}{\Delta_f} \int \delta(f^a(A_\mu^\theta))[d\theta] = 1 . \tag{2.22}$$

and A_μ^θ is the gauge transformation of A_μ. Δ_f^{-1} is called the Faddeev-Popov determinant, and it can be written as

$$\begin{aligned} \Delta_f &= \int \delta(f^a(A_\mu^\theta))[d\theta] , \\ &= 1/\det\left(\frac{\delta(f^a(A_\mu^\theta))}{\delta\theta^b}\right) , \\ &\equiv 1/\det M . \end{aligned} \tag{2.23}$$

Now (2.21) is changed to

$$W \sim \int [d\theta] \int [dA] \delta(f^a(A_\mu)) \exp\left(i \int d^4x \mathcal{L}(x)\right) \det M . \tag{2.24}$$

The integral $\int [dA] \delta(f^a(A_\mu)) \det M$ can be identified as the integral along the hypersurface defined by (2.20), and the integral over $d\theta$ can be recognized as the integral which gives rise to infinity to (2.19). We should therefore throw the θ integral away, and redefine the path integral after gauge fixing to be

$$W_f = \int [dA] \delta(f^a(A_\mu)) \exp\left(i \int d^4x \mathcal{L}(x)\right) \det M . \tag{2.25}$$

Now we want to move the δ-function and the determinant to the exponential. Using the integration identity

$$\det M = \int [dc][d\bar{c}] \exp\left(i \int d^4x d^4y \bar{c}_a(x) M(x,y)_{ab} c(y)_b\right) \tag{2.26}$$

over the Grassman variables c and $\bar{c}$ (known as the ghost fields), the determinant can be moved up to the exponential. For the δ-function, note that the more general gauge fixing condition

$$f^a(A^\mu) = B^a(x) , \tag{2.27}$$

where $B^a(x)$ is an arbitrary function of space and time, does not change the Fadeev-Popov determinant $\det M$ provided

$$\frac{\delta B^a(x)}{\delta\theta^b} = 0 . \tag{2.28}$$

Since all the other terms in W_f are independent of $B^a(x)$, we can put the following integral into W_f as a constant

$$\int [dB] \exp\left(-\frac{i}{2\lambda}\int d^4x B^2(x)\right) , \tag{2.29}$$

(λ is called gauge fixing parameter), and obtain a new vacuum functional which we will denote as W. It is

$$\begin{aligned}
W &= \int [dA][dB]\delta(f^a(A_\mu - B^a)) \exp\left(i\int d^4x[\mathcal{L}(x) - \frac{1}{2\lambda}B^2(x)]\right) \det M \\
&= \int [dA] \exp\left(i\int d^4x[\mathcal{L}(x) - \frac{1}{2\lambda}(f^a(A_\mu))^2]\right) \det M \\
&= \int [dA][d\bar{c}][dc] \exp(i\int d^4x[\mathcal{L}(x) - \frac{1}{2\lambda}(f^a(A_\mu))^2] \\
&\qquad + i\int d^4x d^4y[\bar{c}_a(x) M(x,y)_{ab} c_b(y)]) .
\end{aligned} \tag{2.30}$$

Now remember that the ghost (c and $\bar{c}$) fields introduced in (2.26) are Grassman variables, so they satisfy anti-commutation relations. However, the c-field does not have any Lorentz index, so it must be a scalar field. Hence it violates the usual spin-statistics theorem, and they cannot be physical. In the language of Feynman diagrams, this means that the ghost cannot be an external line, and it must be absent in all tree diagrams. However, there can be internal loop(s) consisting of ghost(s).

It is common to use the covariant gauges, where

$$f^a(A) = \partial^\mu A^a_\mu . \tag{2.31}$$

Then

$$M_{ab}(x,y) = -\partial_\mu (D^\mu)_{ab}\delta^4(x-y) , \tag{2.32}$$

where

$$(D^\mu)_{ab} = \partial^\mu \delta_{ab} + ig(if_{abc})A_c^\mu \tag{2.33}$$

is the covariant derivative for the adjoint representation (compare (2.11)). Inspite of the fact that the covariant derivative depends on the $SU(N)$ representation of the field it works on, for economy we continue to use the same notation D^μ to represent it.

The same formalism can be applied to QED. There, the ghost introduced above is actually decoupled from either the gauge field or the spinor field. Therefore the contribution of the ghost is just a constant, which can be absorbed into the normalization factor, and it is not necessary to consider ghosts in QED at all. However, the language of ghosts will still be useful when we discuss the BRST transformation as well as the gauge invariance of the Green's functions and the scattering amplitudes (see Sec.III).

Having determined the effective Lagrangian density for QED and QCD, we can obtain the Feynman rules from them as shown in Appendix B.

III. VECTOR CURRENT WARD-TAKAHASHI IDENTITY

The conserved current $J^\mu(x) = \bar{\psi}(x)\gamma^\mu\psi(x)$ in QED enables one to derive the *Ward-Takahashi* identity [8] for Green functions. Consider for example a three-point Green function in QED as shown in Fig. 1 . It can be written as

$$G_\mu(x,y,z) = \langle 0|T\left(J_\mu(x)\bar{\psi}(y)\psi(z)\right)|0\rangle\ . \tag{3.1}$$

Under the gauge transformation (2.4) the variation of this Green is proportional to

$$\begin{aligned}
\partial_x^\mu G_\mu(x,y,z) = \partial^\mu[\ & \theta(x^0-y^0)\theta(y^0-z^0)\langle 0|J_\mu(x)\bar{\psi}(y)\psi(z)|0\rangle \\
&+\theta(y^0-x^0)\theta(x^0-z^0)\langle 0|\bar{\psi}(y)J_\mu(x)\psi(z)|0\rangle \\
&+\theta(y^0-z^0)\theta(z^0-x^0)\langle 0|\bar{\psi}(y)\psi(z)J_\mu(x)|0\rangle \\
&-\theta(x^0-z^0)\theta(z^0-y^0)\langle 0|J_\mu(x)\psi(z)\bar{\psi}(y)|0\rangle \\
&-\theta(z^0-x^0)\theta(x^0-y^0)\langle 0|\psi(z)J_\mu(x)\bar{\psi}(y)|0\rangle \\
&-\theta(z^0-y^0)\theta(y^0-x^0)\langle 0|\psi(z)\bar{\psi}(y)J_\mu(x)|0\rangle\ ]\ .
\end{aligned} \tag{3.2}$$

FIGURES

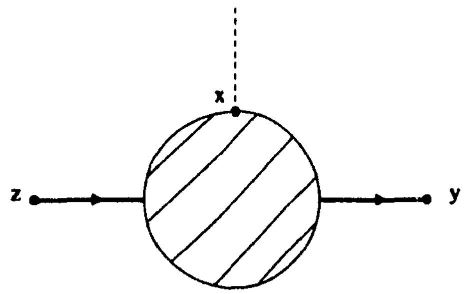

FIG. 1. Three-point Green function. The dots at the ends of the fermion line mean that we include the propagators there.

Using the identity for θ-function

$$\frac{\partial}{\partial x^0}\theta(x^0 - y^0) = \delta(x^0 - y^0)\ , \tag{3.3}$$

and the conservation of the current J_μ, we can simplify the RHS of (3.2) to

$$\partial_x^\mu G_\mu(x,y,z) = \delta(x^0 - y^0)\langle 0|T([J_0(x),\bar{\psi}(y)]\psi(z))|0\rangle + \delta(x^0 - z^0)\langle 0|T(\bar{\psi}(y)[J_0(x),\psi(z)])|0\rangle\ . \tag{3.4}$$

The commutators in (3.4) can be computed using the explicit expression of J_μ, and (2.3). This gives

$$\delta(x^0 - z^0)[J_0(x),\psi_\beta(z)] = -\psi_\beta(z)\delta^4(x - z)\ , \tag{3.5}$$

$$\delta(x^0 - y^0)[J_0(x),\bar{\psi}_\alpha(y)] = \bar{\psi}_\alpha(y)\delta^4(x - y)\ . \tag{3.6}$$

Using this then (3.4) becomes

$$\partial_x^\mu G_\mu(x,y,z) = \delta(x - y)\langle 0|T(\bar{\psi}(y)\psi(z))|0\rangle - \delta(x - z)\langle 0|T(\bar{\psi}(y)\psi(z))|0\rangle\ . \tag{3.7}$$

This is the Ward-Takahashi identity.

Graphically the above identity can be represented as Fig. 2.

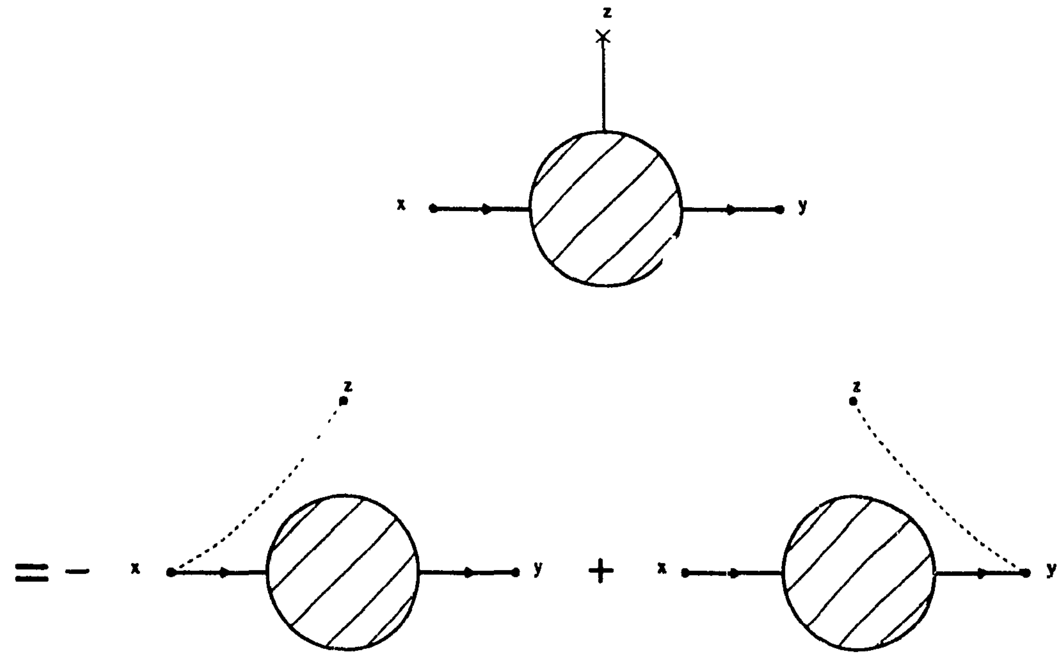

FIG. 2. Ward-Takahashi identity. These diagrams are obtained by sliding the photon line to either end of the fermion line, with an appropriate sign introduced. The cross here means a derivtive ∂_μ(operating on A^μ), and the dots at the ends denote propagators. Thick solid lines, thin solid lines and dashed lines represent fermions(quarks, or electrons), gauge bossons, and ghosts respectively.

Similar identities can be obtained for higher-point Green's functions. Consider, for example, Fig. 3. Then

$$\partial^{x_1}_{\mu_1}\langle 0|T^* \left(J^{\mu_1}(x_1)J^{\mu_2}(x_2)\cdots J^{\mu_n}(x_n)\bar{\Psi}(y)\Psi(z)\right)|0\rangle \ , \tag{3.8}$$

where the T^*-product is the covariant T-product. It differs from the ordinary T-product in having all the commutators between J's removed. The calculation is almost the same as (3.2), and we get

$$\begin{aligned}\partial^\mu_x G_\mu(x,y,z) = &\langle 0|T^* \left(J^{\mu_2}(x_2)J^{\mu_3}(x_3)\cdots J^{\mu_n}(x_n)\bar{\Psi}(y)\Psi(z)\right)|0\rangle\delta^4(x-y) \\ &-\langle 0|T^* \left(J^{\mu_2}(x_2)J^{\mu_3}(x_3)\cdots J^{\mu_n}(x_n)\bar{\Psi}(y)\Psi(z)\right)|0\rangle\delta^4(x-z) \ .\end{aligned} \tag{3.9}$$

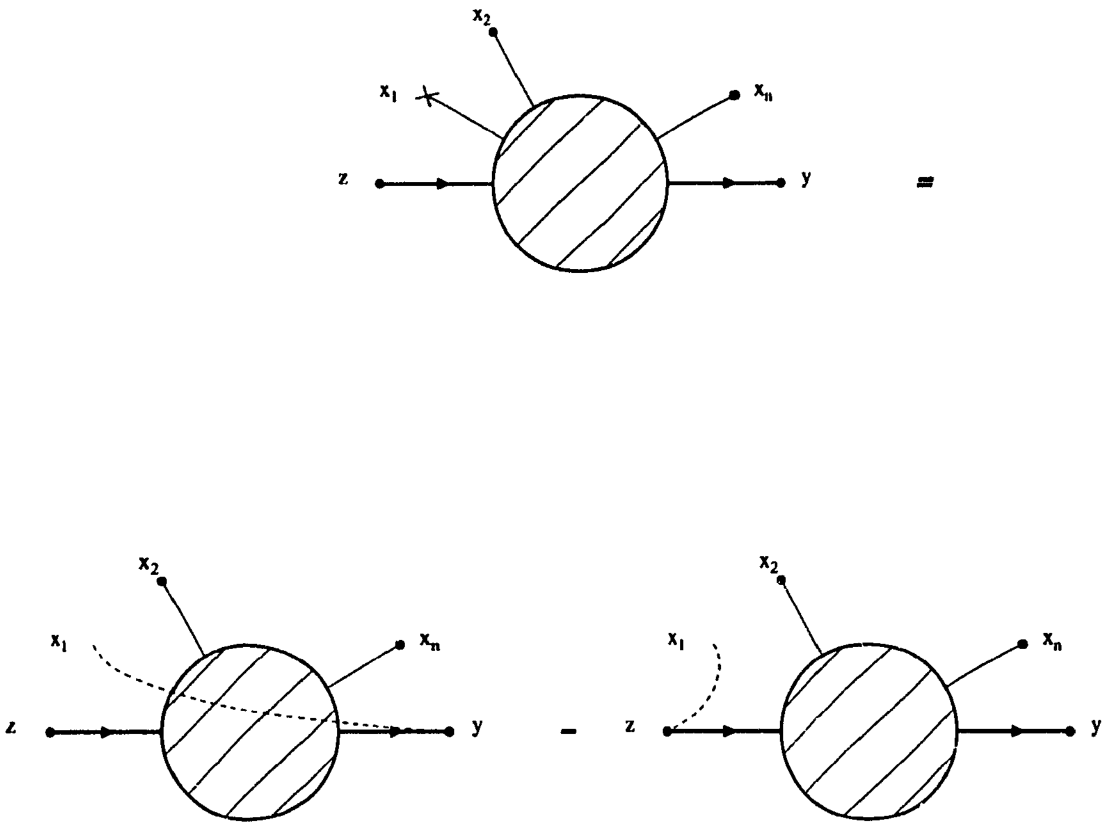

FIG. 3. Ward Takahashi identity for n-point Green's function.

This is the general form of the vector-current Ward-Takahashi identity. It shows the consequence of current conservation on Green's functions. It can also be used to simplify calculations and to show the gauge invariance of the scattering amplitudes. There is another way to derive it, via the so-called BRST invariance which we will discuss in Sec.IV. We shall defer further discussions on the consequences of the Ward-Takahashi identity until then.

IV. BRST TRANSFORMATION

As we saw in Sec.II, a gauge fixing is required to quantize a gauge theory. As a result, the effective Lagrangian density we get is no longer gauge invariant; the local symmetry is broken by the gauge-fixing and the ghost terms. Surprisingly, there is still a remnant global symmetry left in the effective Lagrangian, known as the Becchi-Rouet-Stora-Tyupin (BRST) symmetry [9]. This new symmetry provides a powerful tool to study the consequences of gauge invariance in a gauge theory. One obtains in this way the Slavnov-Taylor identity [10], which is the analogy of the Ward-Takahashi identity in QCD, and is useful in studying the gauge invariance and unitary of the exact scattering amplitudes.

We shall review in the section how the BRST invariance is obtained and some of its applications.

First we consider the effective Lagrangian density without the fermions.

$$\begin{aligned} \mathcal{L} &= -\frac{1}{4}(F^a_{\mu\nu})^2 - \frac{1}{2\lambda}(\partial \cdot A)^2 - \bar{c}^a \partial^\mu D_\mu c^a \ , \\ &\equiv \mathcal{L}_{ga} + \mathcal{L}_{gf} + \mathcal{L}_{gh} \ , \end{aligned} \tag{4.1}$$

where we have chosen the covariant gauges. $\mathcal{L}_{ga}$ is invariant under the gauge transformation

$$\delta A^a_\mu = -\frac{1}{g}\partial_\mu \alpha^a + f^{abc} A^c_\mu \alpha^b = -\frac{1}{g}(D_\mu)^{ab}\alpha^b \ . \tag{4.2}$$

Now we choose a special α

$$\alpha^a = c^a \xi \tag{4.3}$$

where both c^a (ghost field) and ξ are Grassmann variables [6], and ξ is a constant. Then the gauge fixed Lagrangian density (4.1) is invariant under a global transformation

$$\begin{aligned} \delta A^a_\mu &= -\frac{1}{g}(D_\mu c^a)\xi \ , \\ \delta c^a &= -\frac{1}{2} f^{abc} c^b c^c \xi \ , \\ \delta \bar{c}^a &= -\frac{1}{\lambda g}(\partial^\mu A^a_\mu)\xi \ . \end{aligned} \tag{4.4}$$

We can see that the $\mathcal{L}_{ga}$ is invariant because the (4.3) is just a special choice of (2.15). As for the $\mathcal{L}_{gf}$, we have

$$\begin{aligned} \delta \mathcal{L}_{gf} &= \frac{1}{2\lambda}(\partial \cdot A)^2 - \frac{1}{2\lambda}\left[\partial \cdot (A^a - \frac{1}{g}(D_\mu c^a)\xi)\right]^2 \\ &= \frac{1}{2\lambda}(\partial \cdot A)^2 - \frac{1}{2\lambda}\left[(\partial \cdot A)^2 - \frac{2}{g}\partial \cdot A^a \partial^\mu [D_\mu c^a]\xi + \frac{1}{g^2}(D_\mu c^a)^2 \xi^2\right] \ . \end{aligned} \tag{4.5}$$

Remember that ξ is a Grassmann variable, so

$$\xi^2 = 0 \ , \tag{4.6}$$

and we have

$$\delta\mathcal{L}_{gf} = \frac{1}{\lambda g}(\partial^\mu A_\mu^a)(\partial^\nu D_\nu c^a)\xi \ . \tag{4.7}$$

Then $\mathcal{L}_{gh}$ has the following variation

$$\begin{aligned}
\delta\mathcal{L}_{gh} &= \bar{c}^a\partial^\mu D_\mu c^a - (\bar{c}^a + \delta\bar{c}^a)\partial^\mu(D_\mu c^a + \delta D_\mu c^a + D_\mu \delta c^a) \\
&= -\bar{c}^a\partial^\mu\delta(D_\mu c^a) - \delta\bar{c}^a\partial^\mu D_\mu c^a \ , \\
&= -\bar{c}^a\partial^\mu\delta(D_\mu c^a) + \frac{1}{\lambda g}(\partial^\mu A_\mu^a \xi \partial^\nu D_\nu c^a) \ , \\
&= -\bar{c}^a\partial_\mu\delta(D_\mu c^a) - \frac{1}{\lambda g}(\partial^\mu A_\mu^a)(\partial^\nu D_\nu c^a)\xi \ ,
\end{aligned} \tag{4.8}$$

where we have used

$$[\xi, c^a]_+ = 0 \ . \tag{4.9}$$

Therefore we have the variation of the effective Lagrangian density as

$$\begin{aligned}
\delta\mathcal{L} &= \delta\mathcal{L}_{gf} + \delta\mathcal{L}_{gh} \ , \\
&= -\bar{c}^a\partial_\mu\delta(D_\mu c^a) \ .
\end{aligned} \tag{4.10}$$

Recall from (2.16) that

$$D_\mu c^a = \partial_\mu c^a + g f^{abc} A_\mu^b c^c \ , \tag{4.11}$$

we have

$$\begin{aligned}
\delta(D_\mu c^a) &= \partial^\mu(-\frac{1}{2}f^{abc}c^b c^c \xi) + g f^{abc}(-\frac{1}{g}D_\mu c^b)\xi c^c + g f^{abc} A_\mu^b(-\frac{1}{2}f^{cef}c^e c^f)\xi) \\
&= \partial^\mu(-\frac{1}{2}f^{abc}c^b c^c \xi) + g f^{abc} A_\mu^b(-\frac{1}{2}f^{cef}c^e c^f)\xi) + \imath f^{abc}(\partial_\mu c^b)\xi c^c + g f^{abc} f^{bef} c^f A_\mu^e \xi c^c \\
&= 0 \ .
\end{aligned} \tag{4.12}$$

Hence we have proved that the effective Lagrangian density (4.1) is BRST invariant.

When we include the fermion fields in the Lagrangian density, the gauge-fixing term and the ghost contribution remain the same. The BRST transformation of fermions,

$$\begin{aligned} \delta\Psi &= -iT^a c^a \xi \Psi \ , \\ \delta\bar{\Psi} &= i\bar{\Psi} T^a c^a \xi \ , \end{aligned} \tag{4.13}$$

can be considered as the same choice of the gauge transformation as (4.3), hence the following Lagrangian is invariant.

$$\mathcal{L} = \bar{\Psi} i(D_\mu \gamma^\mu - m)\Psi \ . \tag{4.14}$$

Thus the total Lagrangian $\mathcal{L}_{eff}$

$$\mathcal{L}_{eff} = \bar{\Psi} i(D_\mu \gamma^\mu - m)\Psi - \frac{1}{4}(F^a_{\mu\nu})^2 - \frac{1}{2\lambda}(\partial \cdot A)^2 - \bar{c}^a \partial^\mu D_\mu c^a \ , \tag{4.15}$$

is also BRST invariant.

A. BRST invariance and the Ward-Takahashi identity for QED

Let us discuss the Ward-Takahashi identity again. We will now use BRST invariance to get the three-point Green's function identity we obtained before in (3.7).

Consider a trivial three-point Green function

$$\langle 0 | T\left(\psi(x)\bar{c}(y)\bar{\psi}(z)\right) |0\rangle \ . \tag{4.16}$$

We call it trivial because the Green's function above is zero owing to the conservation of ghost numbers. This does not matter because what we want to calculate is its variation under BRST.

$$\delta_{BRST}\langle 0 | T\left(\psi(x)\bar{c}(y)\bar{\psi}(z)\right) |0\rangle = 0 \ . \tag{4.17}$$

Now substitute in the variation of the individual fields from (4.4) and (4.13), then we get a non-trivial identity which will be proved later to be the Ward-Takahashi identity.

$$0 = -i\langle 0|T(\psi(x)c(x)\bar{c}(y)\bar{\psi}(z))|0\rangle + \frac{1}{\lambda e}\langle 0|T(\psi(x)\partial\cdot A(y)\bar{\psi}(z))|0\rangle$$
$$-i\langle 0|T(\psi(x)\bar{c}(y)c(z)\bar{\psi}(z))|0\rangle\ ; \tag{4.18}$$

therefore

$$\langle 0|T(\psi(x)\partial\cdot A(y)\bar{\psi}(z))|0\rangle = -i\lambda e(-\langle 0|T(c(x)\bar{c}(y)\psi(x)\bar{\psi}(z))|0\rangle$$
$$+\langle 0|T(c(z)\bar{c}(y)\psi(x)\bar{\psi}(z))|0\rangle)\ . \tag{4.19}$$

As discussed at the end of Sec.II, the ghost fields are decoupled from the electron and the photon fields in QED. As a result, the ghost fields on the RHS simply pair up to be the free field propagator, so that we have

$$\langle 0|T(\psi(x)\partial\cdot A(y)\bar{\psi}(z))|0\rangle = -i\lambda e(-\langle 0|c(x)\bar{c}(y)|0\rangle\langle 0|T(\psi(x)\bar{\psi}(z))|0\rangle$$
$$+\langle 0|c(z)\bar{c}(y)|0\rangle\langle 0|T(\psi(x)\bar{\psi}(z))|0\rangle)\ . \tag{4.20}$$

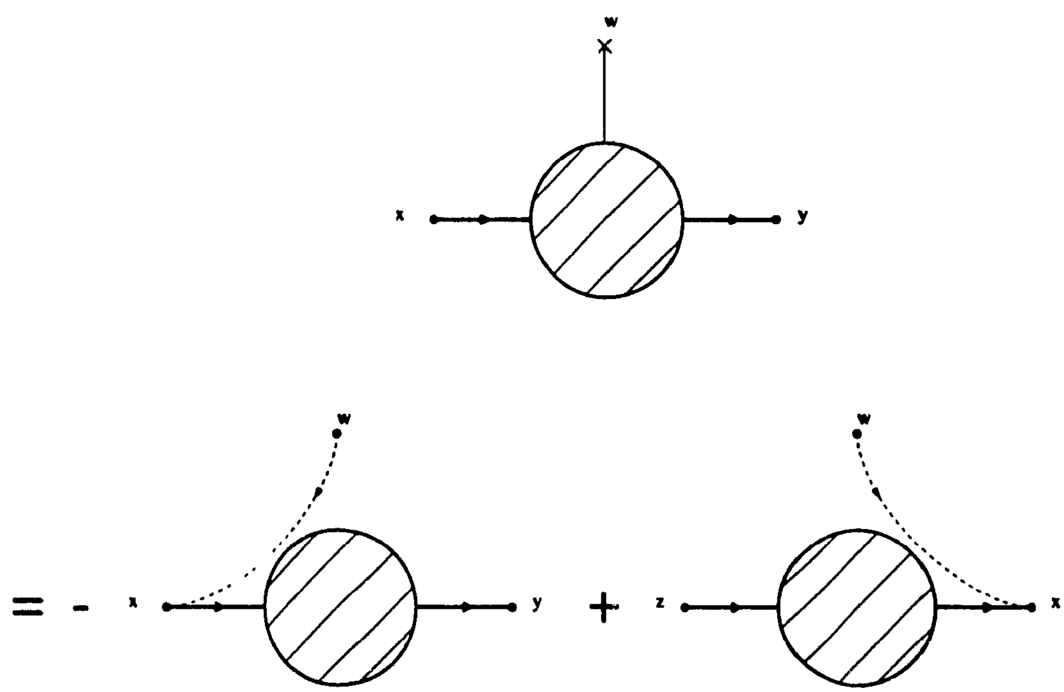

FIG. 4. Ward-Takahashi identity.

This equation can be graphically represented in Fig. 4 ,where a cross in the first graph means a derivative ∂_μ (operating on A^μ), and a dot at the end of a line means that there is a propagator there. We use thick solid lines to denote fermions, i.e. electrons in QED and quarks in QCD. The thin solid lines are used to denote photons or gluons. Dash lines mean ghosts.

By comparing Figs. 4 and Fig. 2, we see that (4.20) is very similar to the Ward-Takahashi identity (3.7), with the first term in (4.20) corresponding to the first term in (3.7), and the second term in (4.20) corresponding to the second terms in (3.7). There are however various superficial differences between the two identities: the LHS of (4.20) contains the field A but not the current J, and the RHS of (4.20) contains additional factors of the ghost propagator functions. However, these additional effects cancel and that results in having the two identities the same. To see that, notice that a Green's function ending with $A(y)$ and a Green's function ending with $J(y)$ simply differ by the presence of a bare photon propagator in the former case, together with a vertex factor ie. In momentum space, this bare propagator is given by

$$\frac{-(g_{\mu\nu} - p_\mu p_\nu/p^2) - \lambda p_\mu p_\nu/p^2}{p^2} \ . \tag{4.21}$$

When we contract this with p^μ, we obtain $-\lambda p_\nu/p^2$, so we can symbolically write $\partial A = -ie\lambda(1/p^2)\partial J$. The $1/p^2$ factor just cancels out with the ghost propagator on the RHS, so we obtain once again the Ward-Takahashi identity (3.7). This BRST way of proving the identity is useful because it is this form that can be generalized relatively easily to non-Abelian gauge theories, as we shall see in the next section.

Generalization to higher-point Green's function is straight forward. Similar to (4.16), we consider the BRST transformation of a trivial Green's function

$$\delta_{BRST}\langle 0|T\left(\psi(x)\bar{c}(y)A^{\mu_1}(w_1)\cdots A^{\mu_n}(w_n)\bar{\psi}(z)\right)|0\rangle \ . \tag{4.22}$$

When we substitute in the variation of the fields, we should remember that we are discussing QED, so the $SU(N)$ color algebra reduces to $U(1)$ algebra. Thus the second term in the RHS of equation (4.11) disappears, and we get the following identity

$$\langle 0|T\left(\psi(x)\partial\cdot A(y)A^{\mu_1}(w_1)\cdots A^{\mu_n}(w_n)\bar{\psi}(z)\right)|0\rangle$$

$$= \lambda e(i\langle 0|T(c(x)\bar{c}(y)\psi(x)A^{\mu_1}(w_1)\cdots A^{\mu_n}(w_n)\bar{\psi}(z))|0\rangle$$

$$-i\langle 0|T(c(z)\bar{c}(y)\psi(x)A^{\mu_1}(w_1)\cdots A^{\mu_n}(w_n)\bar{\psi}(z))|0\rangle$$

$$+\frac{1}{e}\langle 0|T(\partial^{\mu_1}c(w_1)\bar{c}(y)\psi(x)A^{\mu_2}(w_2)\cdots A^{\mu_n}(w_n)\bar{\psi}(z))|0\rangle$$

$$+\frac{1}{e}\langle 0|T(\partial^{\mu_2}c(w_2)\bar{c}(y)\psi(x)A^{\mu_2}(w_1)\cdots A^{\mu_n}(w_n)\bar{\psi}(z))|0\rangle$$

$$+\cdots$$

$$+\frac{1}{e}\langle 0|T(\partial^{\mu_n}c(w_n)\bar{c}(y)\psi(x)A^{\mu_2}(w_1)\cdots A^{\mu_{n-1}}(w_{n-1})\bar{\psi}(z))|0\rangle) \ . \tag{4.23}$$

Taking the connected-diagram part of the above equation, only the first two terms contribute because the rest of them correspond to disconnected diagrams due to the fact that the ghost fields are decoupled from the electron and the photon fields. Therefore we have

$$\langle 0|T(\psi(x)\partial\cdot A(y)A^{\mu_1}(w_1)\cdots A^{\mu_n}(w_n)\bar{\psi}(z))|0\rangle_c$$

$$= -i\lambda e(-\langle 0|c(x)\bar{c}(y)|0\rangle\langle 0|T(\psi(x)A^{\mu_1}(w_1)\cdots A^{\mu_n}(w_n)\bar{\psi}(z))|0\rangle$$

$$+\langle 0|c(z)\bar{c}(y)|0\rangle\langle 0|T(\psi(x)A^{\mu_1}(w_1)\cdots A^{\mu_n}(w_n)\bar{\psi}(z))|0\rangle) \ , \tag{4.24}$$

which can be represented by Fig. 3 too.

When we consider on-shell scattering amplitudes, we must multiply the Fourier transformation of the corresponding Green's function with

$$\prod_{i=1}^{l}(p_i^2 - m_i^2) \tag{4.25}$$

where l is the number of the external particles, and then take the on-shell limit $p_i^2 = m_i^2$. As we can see in Fig.3, each of the diagrams on the RHS has a ghost line attached to an end of the fermion line. This destroys the fermion pole otherwise present so the diagram vanishes after being multiplied by (4.25) and having the on-shell limits taken. This proves the gauge invariance of the exact scattering amplitudes.

B. QCD Slavnov-Taylor identities

Applying the BRST transformation to QCD Green's functions, we obtain the Slavnov-Taylor identities. We will give here a simple example to illustrate it.

First we consider

$$\partial_x^\mu \langle 0|T(\Psi(y)A_\nu^a(z)A_\mu^b(x)\bar{\Psi}(w))|0\rangle \ . \tag{4.26}$$

which is shown in Fig. 5.

To get the identity for this Green function, we must study the BRST variation of another Green function:

$$\delta_{BRST}\langle 0|T(\Psi(y)A_\nu^a(z)\bar{c}^b(x)\bar{\Psi}(w))|0\rangle = 0 \ . \tag{4.27}$$

Write out everything on the LHS of (4.27), we will get the identity we want as follows

$$\begin{aligned}\partial_x^\mu \langle 0|T(\Psi(y)A_\nu^a(z)A_\mu^b(x)\bar{\Psi}(w))|0\rangle = \lambda g (&i\langle 0|T(T^e c^e(y)\bar{c}^b(x)\Psi(y)A_\nu^a(z)\bar{\Psi}(w))|0\rangle \\ &-i\langle 0|T(T^e c^e(w)\bar{c}^b(x)\Psi(y)A_\nu^a(z)\bar{\Psi}(w))|0\rangle \\ &+\frac{1}{g}\langle 0|T(\partial_\nu c^a(z)\bar{c}^b(x)\Psi(y)\bar{\Psi}(w))|0\rangle \\ &+f^{acd}\langle 0|T(c^d(z)\bar{c}^b(x)\Psi(y)A_\nu^c(z)\bar{\Psi}(w))|0\rangle) \ . \end{aligned} \tag{4.28}$$

This can be shown directly by the graphs as in Fig. 5, where as before, a cross indicates a derivative (a divergence when it is on a gluon line, and a gradient when it is on a ghost line). For QCD, the ghost no longer decouples from the other particles. This is indicated in the graphs by having the (dash) ghost lines drawn through the shaded circle, with the implication that interactions with them may take place inside.

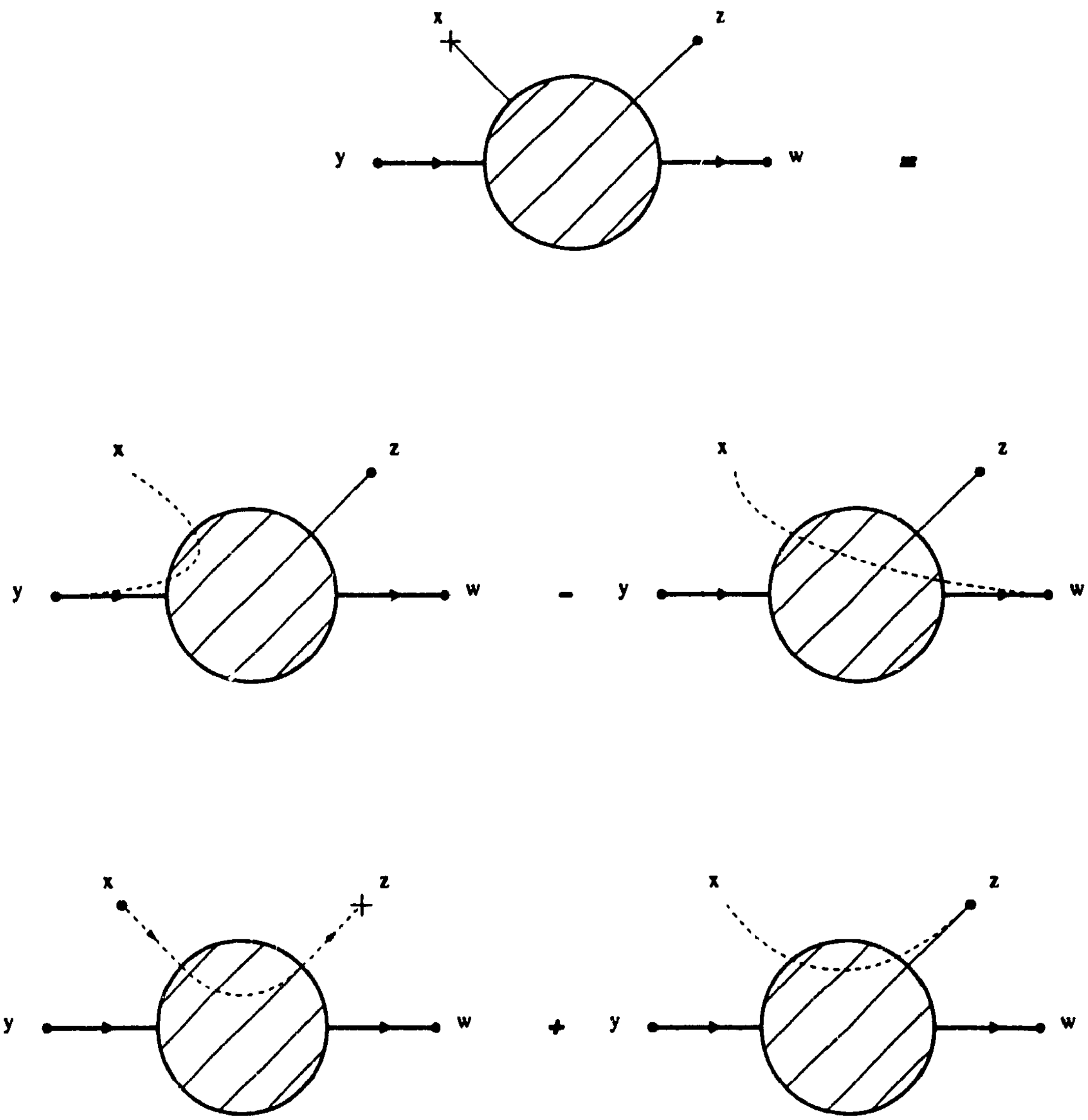

FIG. 5. An example of QCD Slavnov-Taylor identity.

If we consider the corresponding on-shell amplitude, then the first, the second and the last terms on the RHS of (4.28) vanish because of the same reason as before, *i.e.*, the absence of a pole to cancel the Klein-Gordon factor in (4.25). As for the third term, remember that the cross means a derivative, it contains a factor

$$p_z \cdot \epsilon(p_z) = 0 \; . \tag{4.29}$$

Hence the RHS of Fig. 5 vanishes and the on-shell scattering amplitude is gauge invariant.

V. GAUGE INVARIANCE OF PERTURBATIVE AMPLITUDES

We showed in the proceeding section that the exact on-shell scattering amplitudes are gauge invariant. This must persist order-by-order so it follows that the perturbative amplitudes in each order are gauge invariant. However by analysing the perturbative amplitudes in detail, one finds that such invariances are composed of sums of classes of terms each of which is already gauge invariant. It is this refined gauge-invariant property of the perturbative scattering amplitude which we would like to get in this section. Such refined gauge-invariant properties are useful in practical calculations because a separate and convenient gauge choice can be made for a different class, thus allowing the computations to be much simplified.

A perturbative scattering amplitude contains many terms given by a sum of Feynman diagrams. The whole amplitude is gauge invariant but each individual Feynman diagram or each term is not. That is to say, each Feynman diagram contains gauge-dependent terms, and these terms will be canceled when they are summed up in a physical process. But we do not always need to sum up *all* the terms to get gauge invariance. It is sometimes possible to divide the amplitude of a given order into the sum of gauge-invariant subamplitudes. The purpose of this section is to find out how each individual Feynman diagram transforms under a gauge transformation of the wave function of an external gauge particle. For this purpose, we shall use the Feynman gauge ($\lambda = 1$) throughout for gauge propagators. Once the gauge property for a single photon/gluon is known, the gauge property when all the external photons/gluons undergo a simultaneous gauge transformation can be easily obtained.

A. QED perturbative amplitude

To discuss the gauge variation of Feynman diagrams, first look at the variation of the fundamental construction units of a Feynman diagram: the vertices. As we can see in

Appendix A, the QED Feynman rules contain only one kind of vertices. If we introduce gauge transformation to the photon line attached to one of these vertices, its variation can be represented graphically by Fig. 6.

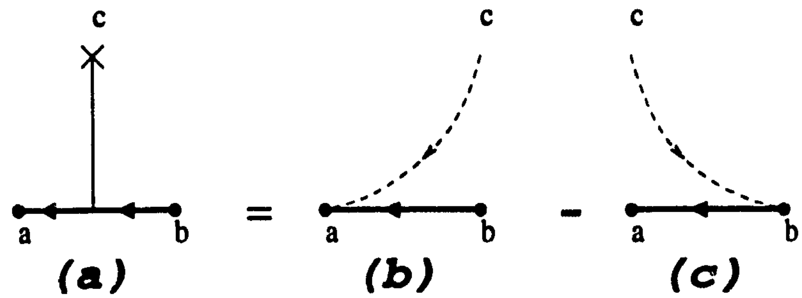

FIG. 6. Variation of a QED vertex.

This can be seen from the BRST technique discussed in the last section, but a direct proof using the Feynman rules can also be given, as follows. The LHS of the Fig. 6 corresponds to the following vertex factor

$$
\begin{aligned}
& ie\left((p_c)^\mu \frac{1}{(p_b+p_c)^\nu\gamma_\nu - m + i\epsilon}\gamma_\mu \frac{1}{p_b^\nu\gamma_\nu - m + i\epsilon}\right) \\
&= ie\left(\frac{1}{(p_b+p_c)^\nu\gamma_\nu - m + i\epsilon}\left((p_b+p_c)^\mu\gamma_\mu - m - (p_b^\mu\gamma_\mu - m)\right)\frac{1}{p_b^\nu\gamma_\nu - m + i\epsilon}\right) \\
&= ie\left(\frac{1}{p_b^\nu\gamma_\nu - m + i\epsilon} - \frac{1}{(p_b+p_c)^\nu\gamma_\nu - m + i\epsilon}\right) .
\end{aligned}
\tag{5.1}
$$

Now we can recognize the two terms in the last line of (5.1) correspond to the two graphs in the RHS of Fig. 6 respectively. The sole purpose of the dashed (ghost) line is to indicate how the momentum p_c is injected into the fermion line.

There are two possibilities of what an end point of the fermion line in the LHS of Fig. 6 can be: a vertex point or an external end. Strictly speaking, for the latter possibility, we should take off the dot at the end, because there is no propagator for an external line.

First, if point a in Fig. 6(a) corresponds to a vertex, then we have a *new* vertex like

Fig. 7(a), obtained from Fig. 6(b).

FIG. 7. (a) is a *new* vertex with vertex factor v_a', (b) is the ordinary vertex with vertex factor v_a. The photon line in both vertices can be either internal or external.

Since the spinor QED vertex factor contains no momenta, the vertex factor v_a' in Fig. 7(a) is equal to v_a in Fig. 7(b).

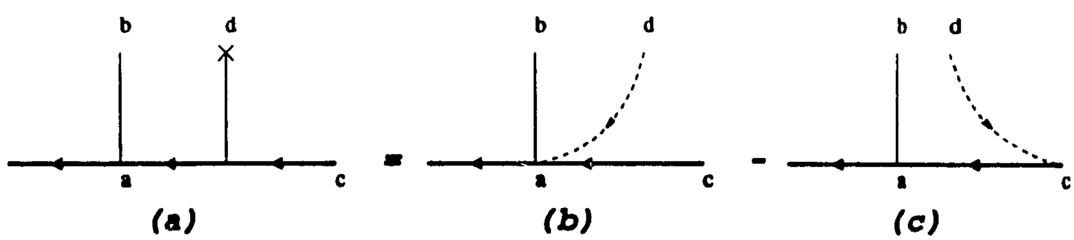

FIG. 8. A graphical identity in QED. We assume that the momentum p_c is incoming and the momentum p_d is outgoing.

Fig. 8 is an example illustrating this fact. Explicitly, its LHS is given by

$$\begin{aligned}
& B' v_a \frac{1}{(p_c^\mu + p_d^\mu)\gamma_\mu - m + i\epsilon} p_d^\nu \gamma_\nu A' \\
&= B' v_a \frac{1}{(p_c^\mu + p_d^\mu)\gamma_\mu - m + i\epsilon} (p_c^\nu \gamma_\nu + p_d^\nu \gamma_\nu - m - (p_c^\nu \gamma_\nu - m)) A' \\
&\to B' v_a' A' = B' v_a A' \; . \qquad (5.2)
\end{aligned}$$

where A' and B' denote all the irrelevant factors, and the arrow in the last step separates out the term corresponding to Fig. 7(a).

Secondly, if point a is an external end, the result of the diagram vanishes because in that case, the fermion propagator is not present to cancel the on-shell Dirac factor $((p_a)^\mu\gamma_\mu - m)$.

We will consider two simple examples to illustrate how Fig. 6 can be used to show directly the gauge invariance of on-shell amplitudes. The first example, shown in Fig. 9, is the Compton scattering amplitude at tree level. The gauge invariance with respect to the first photon line is demonstrated directly in the diagram. A similar proof is valid for the gauge invariance of the second photon line. As a result, the whole amplitude is gauge invariant under a simultaneous gauge transformation of all the lines, but as this example shows, the perturbative proof accomplishes more: we have now demonstrated that gauge invariance is valid separately for each photon line. This very simple example is typical, in the sense that one can obtain more detailed information about gauge invariance by looking directly at the Feynman diagrams.

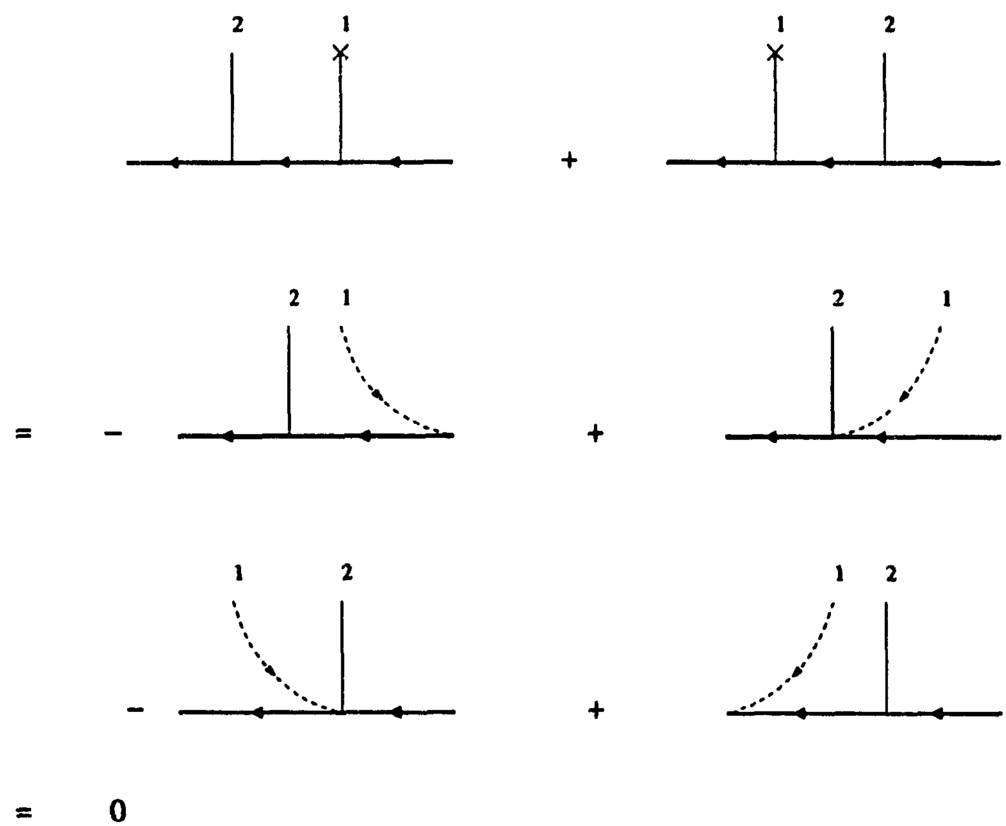

FIG. 9. An example of four-point function at tree level.

The second example, shown in Fig. 10, is a one-loop light-light scattering amplitude. Again the gauge invariance of photon line 4 is demonstrated directly in the diagrams, and the gauge invariance of other photon lines can be proven similarly. Note that as far as the gauge invariance of the line 4 is concerned, it is immaterial whether the other three photon lines are on shell or not, thus making the same proof valid even when these other three photon lines are attached to a much larger diagram.

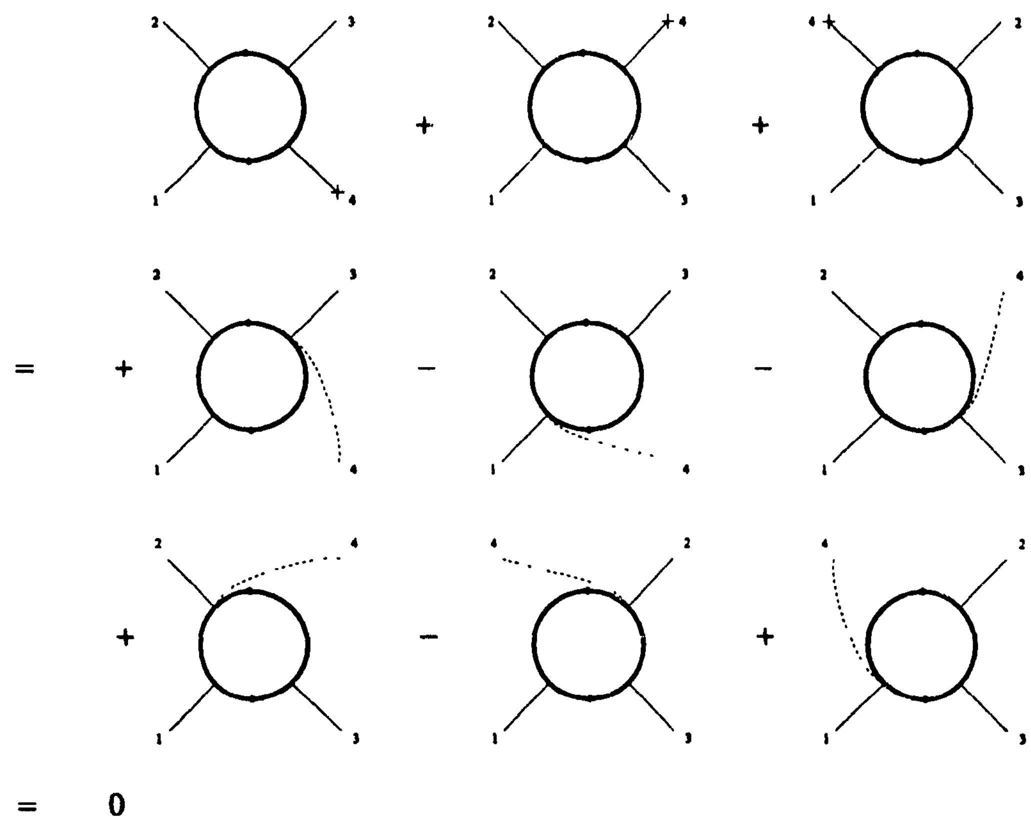

FIG. 10. An example of four-point function at one-loop level.

From these two examples, we can conclude in general that if we introduce gauge transformation to an external photon line, say line a, individual Feynman diagrams are usually gauge dependent; we must sum up a subset of diagrams to get gauge invariance. This subset of diagrams can be obtained by inserting line a in all possible positions along a fermion line, while keeping the other parts of the diagrams unchanged. See Fig. 11 for an illustration.

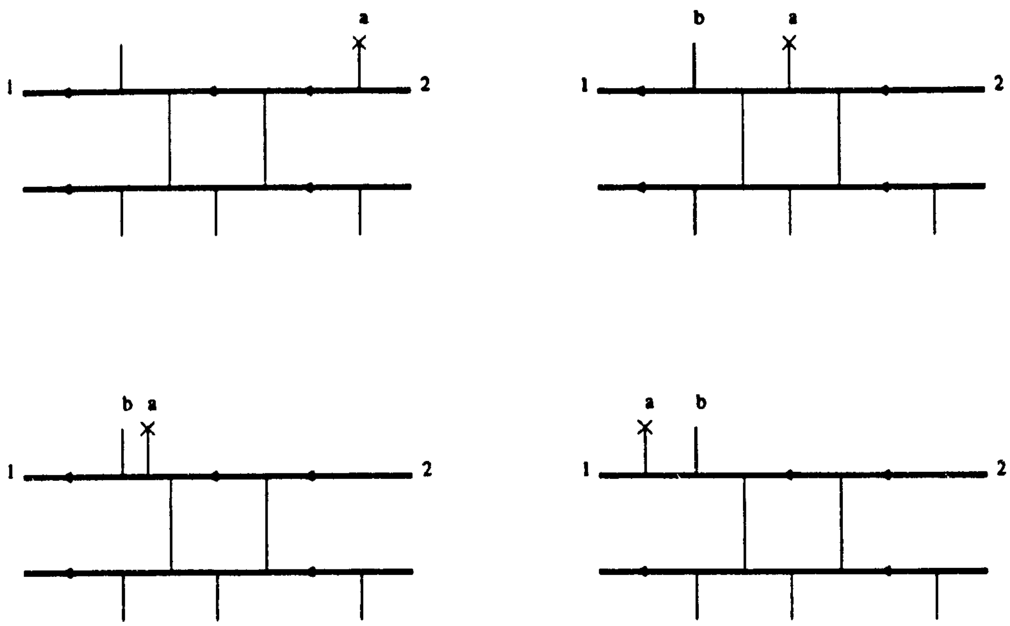

FIG. 11. An invariant subset in QED. As we can see, line a is joined at all possible positions on line 12

A subset of diagrams invariant under gauge transformation of every external photon line can thus be obtained from any Feynman diagram by adding to it all the other diagrams obtained from this one by permuting the photon vertices along each fermion line.

B. Gauge invariance for non-Abelian gauge theories

Non-Abelian gauge theory is more difficult than QED because we have to consider the color (or similar) factor, and more importantly because there are additional vertices in their Feynman rules. We shall confine ourselves in this thesis to $U(N)$ and $SU(N)$ gauge theories, and shall loosely refer to their quantum numbers as 'colors'. For the purpose of considering their gauge invariance, it is simpler first to make a color decomposition of the colored amplitude, as discussed below.

1. color-decomposition

A scattering amplitude, exact or perturbative, contains information on the momentum, spin, and color of the particles involved, and can be written in general as

$$A = \sum_i c_i a_i \ , \tag{5.3}$$

where c_i is the color part and a_i denotes the rest. The amplitude A is gauge invariant, but depending on the choice of c_i, each a_i may not necessary be gauge invariant in general. We would like to show that a proper choice of c_i, in terms of the generalized Chan-Paton factors, will lead to gauge-invariant *subamplitudes* a_i. The Chan-Paton factors were first introduced in open string theory [11], have been used later on in field-theoretical tree-level diagrams [12] [13] as well as one-loop diagrams [14] to simplify calculations. We propose to do this in any number of loops. The full details of the Chan-Paton factor and the general proof for the gauge invariance of a_i will be given in Appendix B. To illustrate how that works, we will discuss the n-gluon amplitude in the tree approximation here in the text.

Let $T^a (a = 0, 1, 2, \cdots, N^2 - 1)$ be the generators of $U(N)$ in the fundamental representation. By deleting T^0 they also form the generators for $SU(N)$. The structure constant f^{abc} in the commutation relation

$$[T^a, T^b] = i f^{abc} T^c \tag{5.4}$$

is fixed by the following normalization which we adopt

$$tr(T^a T^b) = \delta^{ab} \ . \tag{5.5}$$

The corresponding $U(N)$ completeness relation is

$$\sum_{a=0}^{N^2-1} (T^a)_{ij} (T^a)_{kl} = \delta_{il} \delta_{jk} \ . \tag{5.6}$$

As shown in Appendix B, the Chan-Paton factors for a n-gluon amplitude in the tree approximation are given by

$$c_1 = tr(T^1T^2T^3\cdots T^n) , \tag{5.7}$$

and its *non-cyclic* permutations of the n generators inside the trace. The gauge invariance of the colorless subamplitude a_i follows from the independence of c_i. To prove the latter, it is sufficient to show that the various c_i are mutually orthogonal in the large-N limit [15]. For that purpose, let

$$c_i = tr(T^{a_1}T^{a_2}\cdots T^{a_n}) , \tag{5.8}$$

where $\{a_1, a_2, \cdots, a_n\}$ is one of the non-cyclic permutations of $\{1, 2, \cdots, n\}$. These color factors span a vector space, with its dual space being spanned by the dual vectors

$$\tilde{c}_i = tr(T^{a_n}\cdots T^{a_2}T^{a_1}) . \tag{5.9}$$

To get the normalization factor K, defined by $c_i \cdot \tilde{c}_i \equiv \frac{1}{K}\sum_{a_1,a_2,\cdots,a_n} c_i\tilde{c}_i = 1$, we use (5.6) to compute and obtain

$$\begin{aligned} c_i \cdot \tilde{c}_i &= \frac{1}{K}\sum_{a_1,a_2,\cdots,a_n} tr(T^{a_1}T^{a_2}\cdots T^{a_n})tr(T^{a_n}\cdots T^{a_2}T^{a_1}) \\ &= \frac{1}{K}N^n = 1 , \end{aligned} \tag{5.10}$$

thus $K = N^n$.

Now we can prove that the inner product of two different vector vanishes in the large-N limit. For example, consider $c_1 \cdot \tilde{c}_2$ with

$$c_1 = tr(T^1T^2T^3T^4T^5) \; ; \; c_2 = tr(T^2T^3T^5T^4T^1) . \tag{5.11}$$

The normalization factor for them is $K = N^5$, and the inner product is

$$\begin{aligned} c_1 \cdot \tilde{c}_2 &= \sum_{1,2,3,4,5} tr(T^1T^2T^3T^4T^5)tr(T^1T^4T^5T^3T^2)\frac{1}{K} \\ &= \frac{N^3}{N^5} \\ &= 0 . \end{aligned} \tag{5.12}$$

In other words, unless the order of the indices match, as between c_i and $\tilde{c}_i$, otherwise we will have less power of N in the numerator than the denominator, and the dot product $c_i \cdot \tilde{c}_j$ would vanish at the infinite-N limit. This statement is true also for multi-loop cases, which will be proved in Appendix B.

2. color-oriented diagrams

As we mentioned in the last subsection, a scattering amplitude in QCD can be decomposed into gauge-invariant subamplitudes, each of which corresponds to a different color factor. To study this color subamplitude, a simple way is to use the color-oriented diagrams [4].

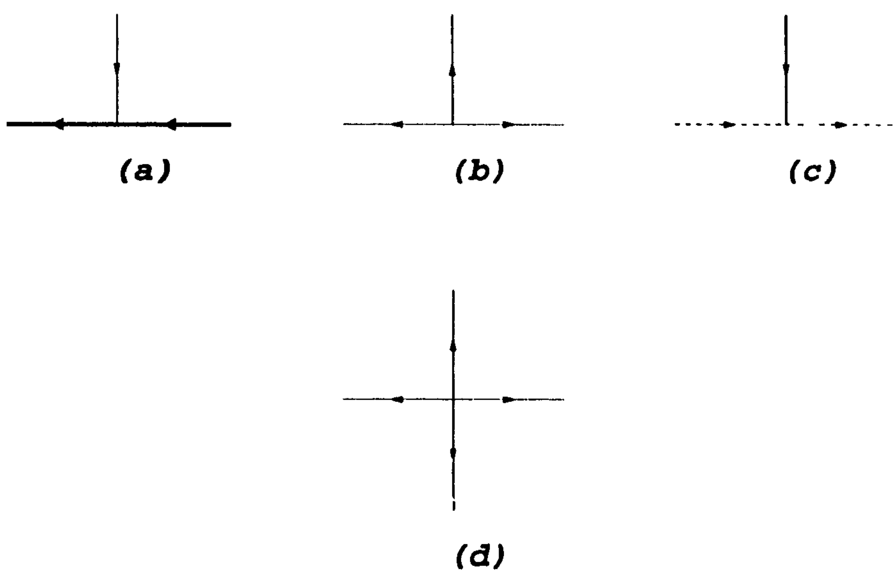

FIG. 12. Ordinary vertices in QCD

The main idea for color-decomposition is to divide a Feynman diagram into different parts according to their color factor. To do so we start with vertices, the basic elements of a diagram. For the gluon-quark vertex (Fig. 12(a)), it is not necessary to decompose it, and the oriented vertex (Fig. 13(i)) is the same as the ordinary vertex. The color factor for a triple-gluon vertex (Fig. 12(b)) is f^{abc}, which can be decomposed into two terms

$$f^{abc} = -i\left(tr(T^aT^bT^c) - Tr(T^aT^cT^b)\right) \ , \tag{5.13}$$

so an ordinary triple-gluon vertex can be represented by two color-oriented vertices (Fig. 13(ii,iii)), differing from one another by the clockwise ordering of their color indices. Similarly for the ghost-gluon vertex (Fig. 12(c)), we get the two oriented vertices as shown in Fig. 13(iv,v).

As for the four-gluon vertex (Fig. 12(d)), the color factor is

$$f^{abe}f^{ecd} = (-i)^2(Tr(T^aT^bT^cT^d) - Tr(T^bT^aT^cT^d) - Tr(T^aT^bT^dT^c) + Tr(T^bT^aT^dT^c)) \ , \tag{5.14}$$

and we need four oriented vertices (Fig. 13(vi,vii,viii,ix)) to represent it.

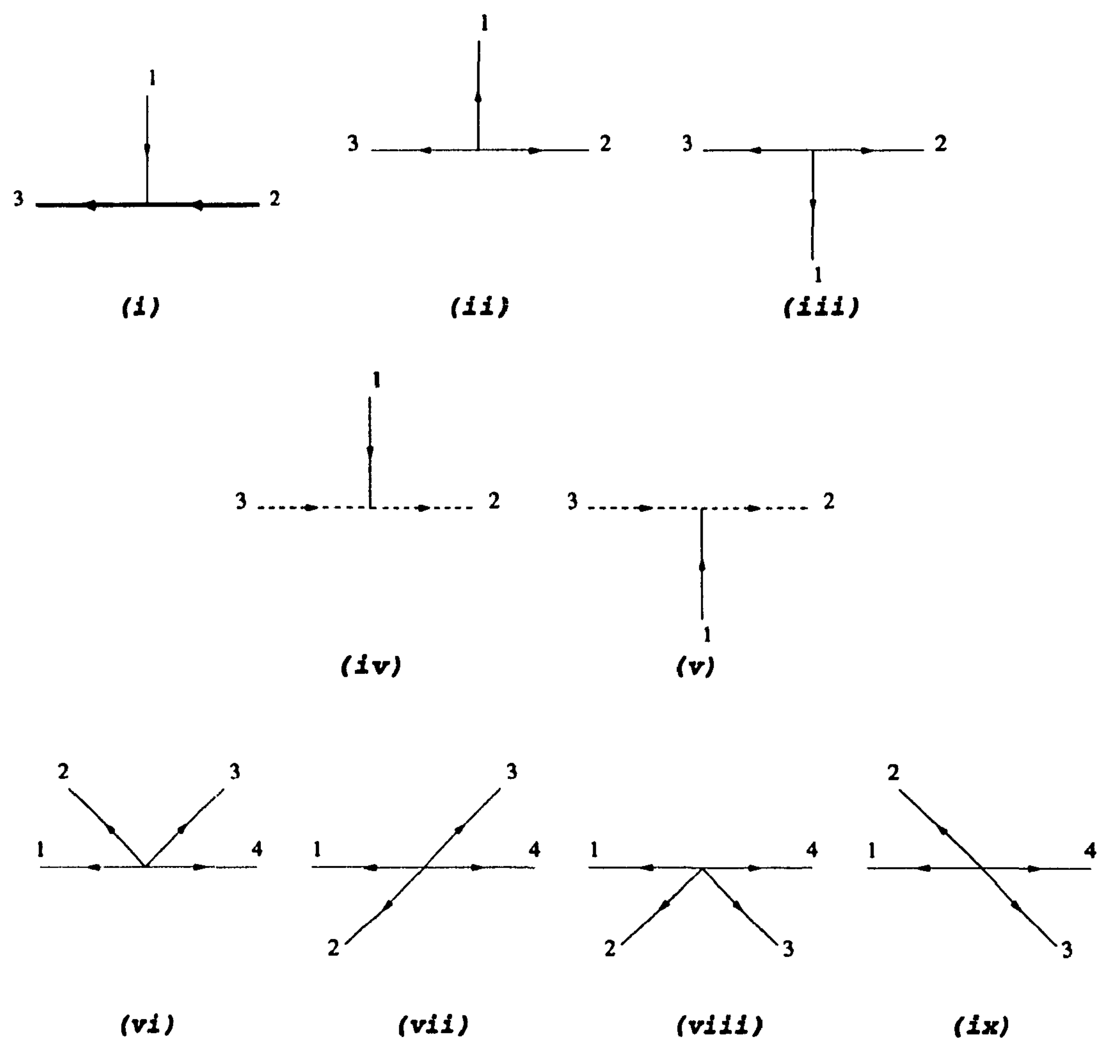

FIG. 13. Oriented vertices for QCD. The line labelled 1 carries a momentum p_1, color factor a, and a space-time index α, while the line 2 carries p_2, b, and β, etc.

The vertex factors for these color oriented vertices are:

- (i) $ig(T^a)_{cb}(\gamma_\alpha)_{\gamma\beta}$;
- (ii) $gtr(T^aT^bT^c)(g_{\beta\gamma}(p_2-p_3)_\alpha + g_{\gamma\alpha}(p_3-p_1)_\beta + g_{\alpha\beta}(p_1-p_2)_\gamma)$;
- (iii) $gtr(T^bT^aT^c)((g_{\beta\gamma}(p_2-p_3)_\alpha + g_{\gamma\alpha}(p_3-p_1)_\beta + g_{\alpha\beta}(p_1-p_2)_\gamma)$;
- (iv) $-gtr(T^aT^bT^c)(p_2)_\alpha$;
- (v) $-gtr(T^bT^aT^c)(p_2)_\alpha$;
- (vi) $ig^2tr(T^aT^bT^cT^d)(-g_{\beta\gamma}g_{\alpha\delta} - g_{\alpha\beta}g_{\gamma\delta} + 2g_{\alpha\gamma}g_{\beta\delta})$;
- (vii) $ig^2tr(T^aT^cT^dT^b)(-g_{\beta\gamma}g_{\alpha\delta} - g_{\alpha\beta}g_{\gamma\delta} + 2g_{\alpha\gamma}g_{\beta\delta})$;
- $(viii)$ $ig^2tr(T^aT^dT^cT^b)(-g_{\beta\gamma}g_{\alpha\beta} - g_{\alpha\beta}g_{\gamma\delta} + 2g_{\alpha\gamma}g_{\beta\delta})$;
- (ix) $ig^2tr(T^aT^bT^dT^c)(-g_{\beta\gamma}g_{\alpha\gamma} - g_{\alpha\beta}g_{\gamma S} + 2g_{\alpha\gamma}g_{\beta\delta})$;

By joining these color-oriented vertices together we get a color-oriented diagram. As the color-oriented vertices are just the decomposition of the ordinary vertices, the total contribution to a Feynman diagram is just the sum of all the possible oriented diagrams for that Feynman diagram.

To get the color factor for an oriented diagram, we multiply all the color factors of the color oriented vertices, and sum over the intermediate color indices. The following two identities coming from the completeness relation (5.6),

$$\sum_{a=0}^{N^2-1} tr(T^aX)tr(T^aY) = tr(XY) \ , \tag{5.15}$$

$$\sum_{a=0}^{N^2-1} tr(T^aXT^aY) = tr(X)tr(Y) \ , \tag{5.16}$$

can be used to obtain the Chan-Paton factor of an oriented diagram. For example, in Fig. 14(a), the color factor becomes

$$\sum_{a=0}^{N^2-1} tr(T^aT^bT^c)tr(T^cT^dT^f) = tr(T^aT^bT^dT^f) \ . \tag{5.17}$$

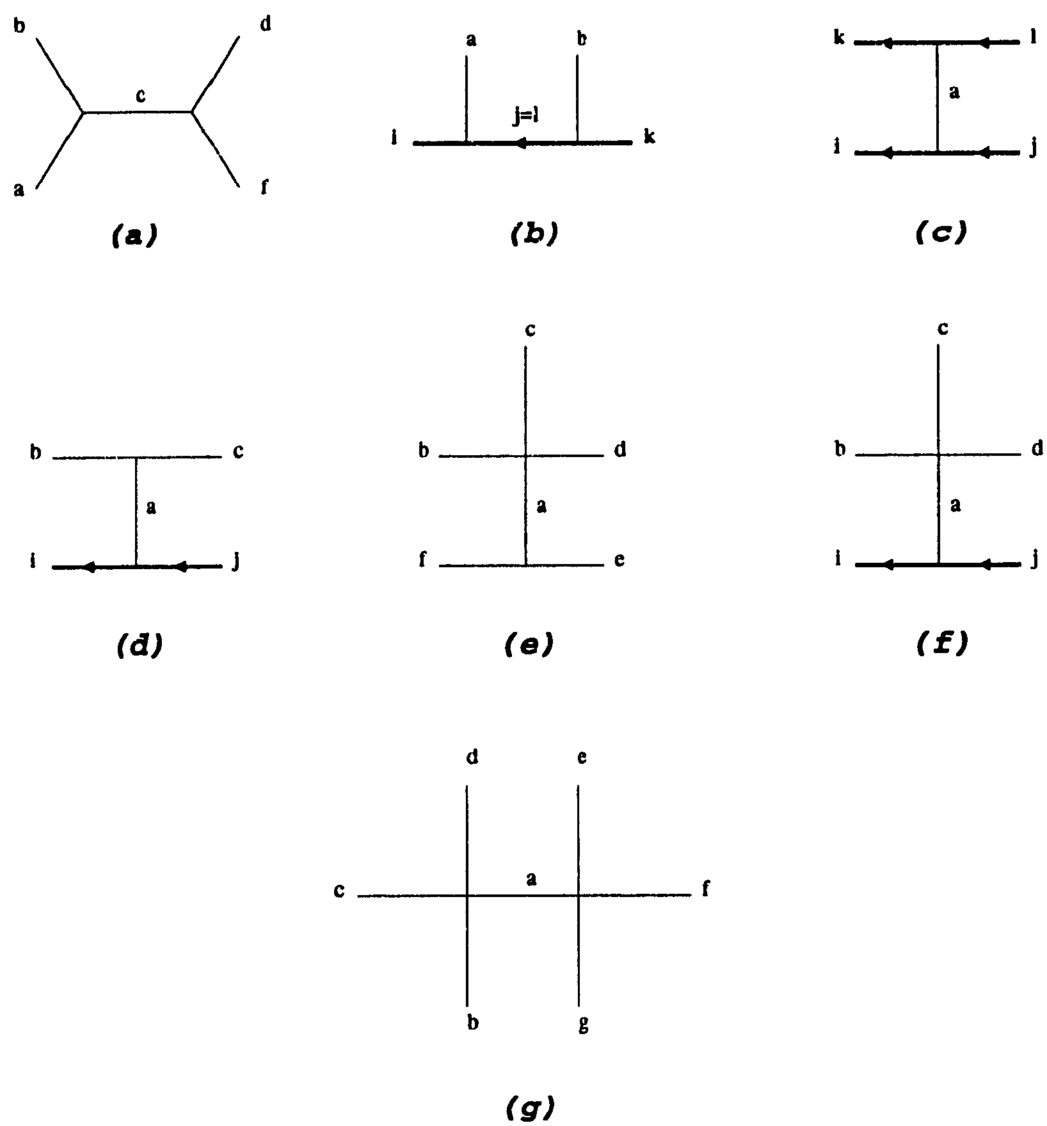

FIG. 14. A color-oriented diagram. The indices are the color indices

To join together two adjacent quark-gluon vertices on the same fermion line, as in Fig. 14(b) , we use

$$T^a_{ij}\delta_{jl}T^b_{lk} = (T^aT^b)_{ik} \ , \tag{5.18}$$

where the δ-function comes from the quark propagator between those two vertices. That means in order to calculate the color factor of a diagram with several external gluons joined to a quark line, we simply multiply all the generators along the quark line in the same order as they are found in the diagram, and then take the ij matrix element, where ij are determined by the external quark wave-functions.

To join together two non-adjacent quark-gluon vertices, or two vertices on different quark lines, as in Fig. 14(c) , we use the $U(N)$ relation

$$\sum_{a=0}^{N^2-1} (T^a)_{ij}(T^a)_{kl} = \delta_{il}\delta_{jk} \ . \tag{5.19}$$

Graphically, when we multiply all the generators along a quark line as described above, then this means that when we encounter a gluon line we should pass through it to onto the other quark line.

If we join an oriented triple gluon vertex with an oriented gluon-quark vertex as shown in Fig. 14(d), we obtain a color factor

$$\begin{aligned} \sum_{a=0}^{N^2-1} (T^a)_{ij} tr(T^aT^bT^c) &= (\sum_{a=0}^{N^2-1} (T^a)_{ij}(T^a)_{kl})(T^b)_{lm}(T^c)_{mk} \ , \\ &= (T^bT^c)_{ij} \ . \end{aligned} \tag{5.20}$$

Now comes the four-gluon vertex. If we join an oriented four-gluon vertex with an oriented tiiple-gluon vertex as shown in Fig. 14(e), we have

$$\sum_{a=0}^{N^2-1} tr(T^aT^bT^cT^d)tr(T^aT^eT^f) = tr(T^bT^cT^dT^eT^f) \ . \tag{5.21}$$

If we join it with a gluon-quark vertex as shown in Fig. 14(f), then the color factor is

$$\sum_{a=0}^{N^2-1} tr(T^aT^bT^cT^d)(T^a)_{ij} = (T^bT^cT^d)_{ij} \ . \tag{5.22}$$

where we have used the completeness relation.

When a four-gluon vertex is connected to another four-gluon vertex as in Fig. 14(g),

$$\sum_{a=0}^{N^2-1} tr(T^aT^bT^cT^d)tr(T^aT^eT^fT^g) = tr(T^bT^cT^dT^eT^fT^g) \ . \tag{5.23}$$

The color factor for the ghost-gluon vertex is the same as the triple-gluon vertex, and the argument is also the same.

Using these arguments inductively, we can prove the following rules, which allow us to read off the color factor of an oriented diagram directly. It is worthwhile to study these graphic rules here, because later on when we use BRST transformation to discuss the gauge invariance of QCD perturbative scattering amplitudes, these rules can help to bypass tedious algebra.

After ref [4], first we define some notations.

A *color path* is a continuous path along the lines of an color-oriented diagram. There are two kinds of paths, open path and closed path. An open path starts with an incoming quark line, and ends at an outgoing quark line. A closed path starts with an external gluon and comes back to this external gluon finally to complete a trace. For both paths, the following must be satisfied:

1. each quark line can be passed at most once, and each gluon line as well as each ghost line can be traversed at most twice;

2. the path must go along the arrow when a quark line is transversed;

3. when a gluon-quark vertex is encountered, path along a quark line turns to follow the gluon line and vice versa;

4. the ghost-gluon vertex here can be treated as a triple-gluon vertex.

5. turn to the leftmost gluon line when a four-gluon or triple gluon vertex is encountered.

Construct all possible color paths so that each quark line of the diagram is passed by once and each ghost line and each gluon line is traversed twice. The union of these color paths then determine the overall color factor of the oriented diagram, as we shall see later.

In practical calculations, it is more convenient to construct all the open paths before the closed paths.

After we get all the paths, we can begin to write the color factor for each path. A closed path corresponds to a trace,

$$tr(T^a T^b \cdots T^n) \ , \tag{5.24}$$

where $a, b, \cdots, n$ are the color indices of the external gluon lines, written from left to right according to the order that the path encounters them.

An open path will be a color matrix element

$$(T^a T^b T^c \cdots T^n)_{ij} \ , \tag{5.25}$$

where $a, b, \cdots, n$ are ordered according to the path as before, and i, j are the color index of the outgoing quark and the incoming quark lines respectively.

Finally, the overall color factor for the oriented diagram is given by the product of the color factors of the individual paths. To check these rules, we present two examples here.

The first one is shown in Fig. 15. We calculate the color factor directly to check the consistency and to compare the efficiency. the generator T^a will be abbreviated by its color index a below.

$$\begin{aligned} C &= \sum_{b,d,f,h,j,l} tr(lab)tr(bdc)tr(def)tr(fhg)tr(hij)tr(jlk) \\ &= tr(ladc)tr(def)tr(fhg)tr(hij)tr(jlk) \\ &= tr(claef)tr(gfilk) \\ &= tr(gclaeilk) \\ &= tr(aci)tr(kgc) \ . \end{aligned} \tag{5.26}$$

From this example, we can see that the first trace corresponds to the outer circle around the loop, while the second one corresponds to the inner circle. The outer circle is clockwise, and the inner one is anti-clockwise. This agrees with the rules, because if we start with line a, we will turn to line b first, and get the first color path as

$$v1 = (abdefhijl) \tag{5.27}$$

which corresponds to

$$c_{v1} = tr(aei) \ . \tag{5.28}$$

And when we start with line c, the left most line we will choose is line b. The second color path is

$$v2 = (cblkjhgfd) \tag{5.29}$$

which means

$$c_{v2} = tr(kgc) \ . \tag{5.30}$$

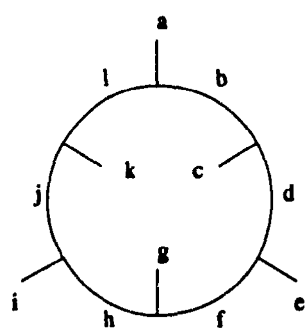

FIG. 15. An example for the color-oriented diagram

The second example as shown in Fig. 16 is much more complicated, and we should use the graphic rules directly. The complete set of color paths are

$$\begin{aligned} v1 &= (1,9,10,11,12,2,13,17,3,18,19,20,21,26,4) \ , \\ v2 &= (5,10,16,14,17,18,24,23,21,25,26,22,9) \ , \\ v3 &= (11,16,15) \ , \\ v4 &= (7,19,24,6,23,8,20) \ , \\ v5 &= (14,13,12) \ . \end{aligned} \tag{5.31}$$

The corresponding color factors are

$$\begin{aligned} C_{v1} &= (T^2T^3)_{14} \ , \\ C_{v2} &= tr(T^5T^{25}) \ , \\ C_{v3} &= tr(1) \ , \\ C_{v4} &= tr(T^6T^8T^7) \ , \\ C_{v5} &= tr(1) \ . \end{aligned} \tag{5.32}$$

Therefore the color factor for this color-oriented diagram is

$$\begin{aligned} C &= C_{v1}C_{v2}C_{v3}C_{v4}C_{v5} \ , \\ &= (T^2T^3)_{14}tr(T^5T^{25})tr(1)tr(T^6T^8T^7)tr(1) \ . \end{aligned} \tag{5.33}$$

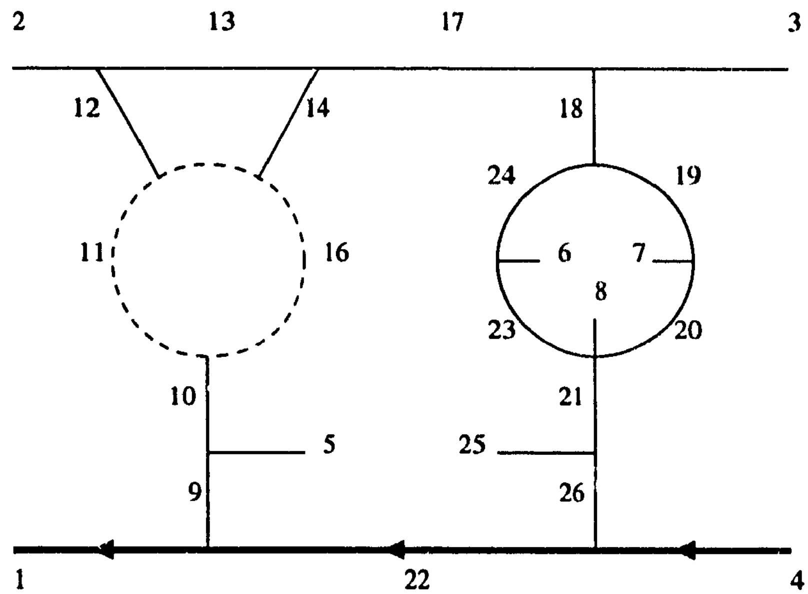

FIG. 16. An other example for the color-oriented diagram

For most of this section we have concentrated on the $U(N)$ gauge theories. Similar results and rules can be developed for $SU(N)$ but they tend to be a bit more complicated. To start with, $tr(T^a) = 0$ for the $SU(N)$ generators T^a so some of the independent color factors c_i in $U(N)$ may be zero or may be mutually related in $SU(N)$. Moreover, to obtain the $SU(N)$ completeness relation, we must move the $a = 0$ term of (5.6) to the RHS, as a result of which a color-oriented diagram will generally contain more than one color factors. One of these color factors will still be the one discussed above for $U(N)$, but in addition there are other factors as well. Nevertheless, we will show in the next section that the sum of all the amplitudes for the color-oriented diagrams with the same $U(N)$ color factor is gauge invariant, and that this result is true irrespective of whether the underlying gauge theory is

$U(N)$ or $SU(N)$, because color itself does not enter into that proof at all.

C. QCD perturbative amplitude — vertex variations

In this subsection we consider how each of the non-Abelian vertices varies under a gauge transformation. The results so obtained are then assembled to give us the variation of a color-oriented diagram.

Our general procedure will be to use the BRST invariance to suggest the relevant terms resulting from such a variation of each vertex. We will then go back to the color-oriented Feynman rules for that vertex to derive the exact factors associated with each of the BRST diagrams for the variations.

To simplify the expression, from now on we will use $(1, 2, \ldots,)$ to replace the space-time indices $(\alpha, \beta, \cdots,)$.

1. *quark-gluon vertex*

The variation of the quark-gluon vertex is similar to the variation of the photon-electron vertex in QED.

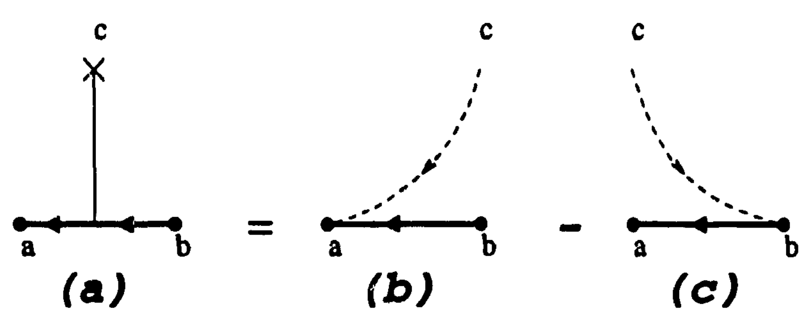

FIG. 17. Variation of a quark-gluon vertex.

Note the rule for the signs of these diagrams. If the ghost line slides to the end of the fermion line (Fig. 17(b)), it has a plus sign. If the ghost line slides to the beginning of the fermion line (Fig. 17(c)), it has a negative sign.

2. triple-gluon vertex

From $\delta_{BRST}\langle 0|T(A_\mu(x)\bar{c}(y)A_\nu(z))|0\rangle = 0$, it follows that

$$\langle 0|T(D_\mu c\xi\bar{c}A_\nu)|0\rangle + \langle 0|T(A_\mu\bar{c}D_\nu c\xi)|0\rangle + \frac{1}{\lambda}\langle 0|T(A_\mu\partial\cdot A\xi A_\nu)|0\rangle$$
$$= 0 \,, \qquad (5.34)$$

or more precisely,

$$\langle 0|T(A_\mu\partial\cdot AA_\nu)|0\rangle = -\lambda(\langle 0|T(\partial_\mu c\bar{c}A_\nu)|0\rangle + gf^{abc}T^a\langle 0|T(A^b_\mu c^c\bar{c}A_\nu)|0\rangle$$
$$+\langle 0|T(A_\mu\bar{c}\partial_\nu c)|0\rangle + f^{abc}T^a g\langle 0|T(A_\mu\bar{c}A^b_\nu c^c)|0\rangle) \,. \qquad (5.35)$$

This suggests the following graphical identity.

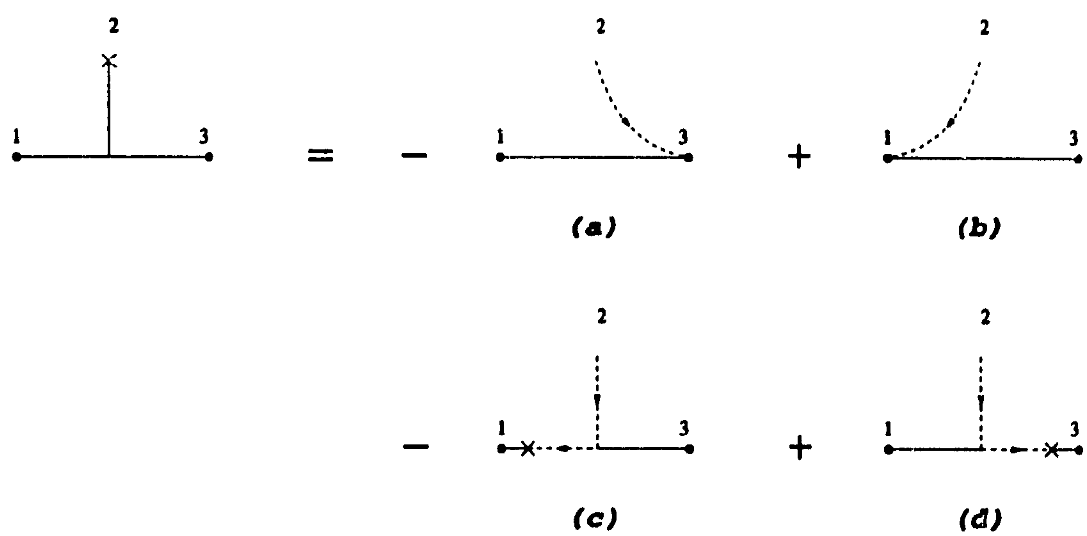

FIG. 18. Variation of a triple gluon vertex

It is not very simple to apply this identity directly. Among other things, one must remove the external gluon line as was done in an analogous case in QED. Instead, it is much simpler to start from the color-oriented Feynman rules and arrange the results of their gauge variations into these BRST diagrams. This is the general procedure which we will adopt for all the vertices. The result of a gauge variation of the second gluon line can be read off from Fig. 13 to be

$$
\begin{aligned}
& g(p_2)_2\left(g_{12}(p_1 - p_2)_3 + g_{23}(p_2 - p_3)_1 + g_{13}(p_3 - p_1)_2\right) \\
&= g\left((p_2)_1(p_1 - p_2)_3 + (p_2)_3(p_2 - p_3)_1 - g_{13}(p_3^2 - p_1^2)\right) \\
&= g\left((p_2)_1(p_1)_3 - (p_2)_3(p_3)_1 - g_{13}(p_3^2 - p_1^2)\right) \\
&= g\left((-p_1 - p_3)_1(p_1)_3 - (-p_1 - p_3)_3(p_3)_1 - g_{13}p_3^2 + g_{13}p_1^2\right) \\
&= g\left(-(p_1)_1(p_1)_3 + (p_3)_3(p_3)_1 - g_{13}p_3^2 + g_{13}p_1^2\right) \ . \qquad (5.36)
\end{aligned}
$$

These four terms can be summarized in the four diagrams above, in Figs. 18((c), (d), (a), (b)), respectively. The $(p_1)_1$ factor in the first term is represented by the cross at the end of the ghost line, and the $(p_1)_3$ factor is present on account of the ghost-gluon vertex. Similar correspondence can be seen between the second term and Fig. 18(d). The p_3^2 factor in term 3 corresponds to the absence of the corresponding gluon propagator in Fig. 18(a), and similarly the factor p_2^2 of the last term corresponds the absence of the gluon propagator on the other side as shown in Fig. 18(b).

We shall call diagrams (Fig. 18(a) and (b)) above the *sliding diagrams*. Similarly, the diagrams on the RHS of rule 1 are also sliding diagrams. On the other hand, diagrams Fig. 18(c) and (d) are obtained by substituting the longitudinal gluon line (that with a cross) by a ghost line. We shall refer to them as *substitution diagrams*. Note that these ghost lines can turn into a gluon line half way down a propagator without any penalty, and the resulting mixed-ghost-gluon propagator should still be treated as a pure gluon propagator.

Each diagram carries a sign as shown. For the sliding diagrams, the sign is determined by the relative orders of three points: the end point of the ghost line,the end point of the gluon line, and the joining point of these two lines. If these three points are in clockwise orderas in Fig. 18(b), then the sign is positive. If they are in anti-clockwise order, then the sign is negative. For the substitution diagrams, the sign is positive if the cross turns left, and negative if it turns right. However, it turns out that the absolute signs of these substitution diagrams are never important.

3. ghost vertex

The BRST variation

$$\delta_{BRST}\langle 0|T(\bar{c}\bar{c}c)|0\rangle = 0 \;, \tag{5.37}$$

suggests the following diagrams.

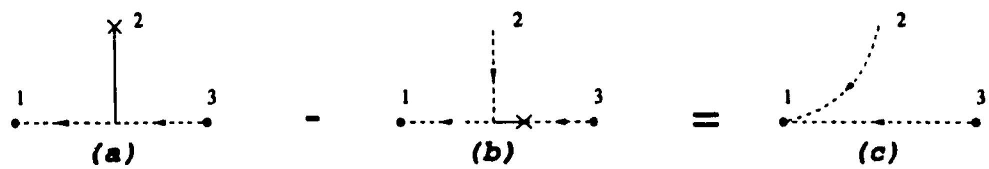

FIG. 19. Gauge variation of a ghost vertex.

From the explicit Feynman rules, one computes Fig. 19(a) to get

$$\begin{aligned} &-g(p_2)_2(p_1)_2 g_{13} \\ &= -g(p_1 \cdot p_2) g_{13} \\ &= -g(-p_1^2 - p_1 \cdot p_3) g_{13} \\ &= g(p_1^2 + p_1 \cdot p_3) g_{13} \;. \end{aligned} \tag{5.38}$$

This corresponds to Figs. 19(c) and 19(b) respectively.

4. four-gluon vertex

The new vertex Fig. 20(a) would result for example by applying rule 1 to Fig. 20(b).

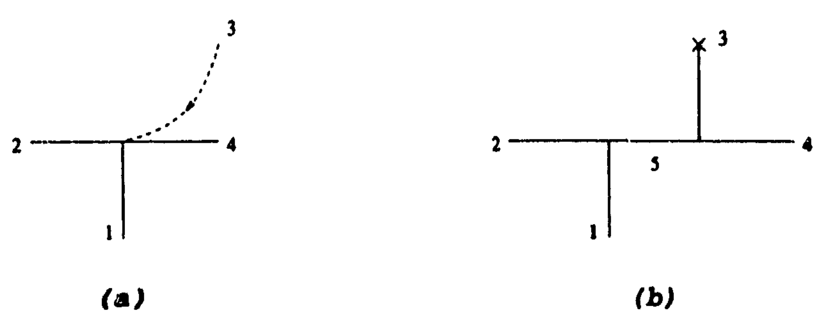

FIG. 20. (a) a new vertex; (b) the original one.

The vertex factor for this diagram is

$$
\begin{aligned}
& ig^2(g_{12}(p_1 - p_2)_5 + g_{25}(p_2 - p_5)_1 + g_{51}(p_5 - p_1)_2)p_5^2 g_{45}\frac{1}{p_5^2} \\
&= ig^2 g_{12}(p_1 - p_2)_4 + g_{24}(p_2 - p_5)_1 + g_{41}(p_5 - p_1)_2 \,, \qquad (5.39)
\end{aligned}
$$

Using momentum conservation,

$$p_5 = p_3 + p_4 \,. \qquad (5.40)$$

we get

$$ig^2 g_{12}(p_1 - p_2)_4 + g_{24}(p_2 - p_3 - p_4)_1 + g_{14}(p_3 + p_4 - p_1)_2 \,. \qquad (5.41)$$

This is just the triple-gluon vertex except that the momentum p_4 is now replaced by $p_3 + p_4$. In other words, as before, the ghost line does nothing except to inject some momentum. We draw line 3 in such a funny way to indicate its pairing with line 4, as the following diagrams are not the same.

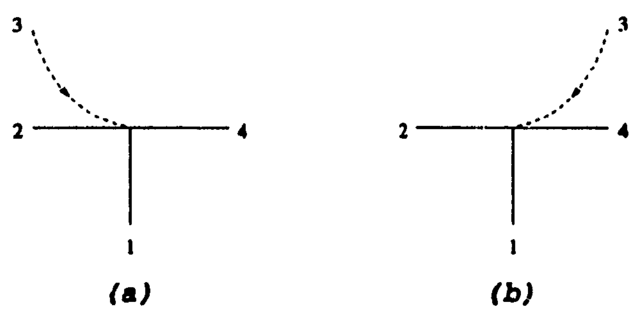

FIG. 21. Two different vertices.

Using the same discussion as above we can find out the vertex factor for the Fig. 21(a) is

$$ig^2 g_{12}(p_1 - p_2 - p_3)_4 + g_{24}(p_2 + p_3 - p_4)_1 + g_{41}(p_4 - p_1)_2 \,. \qquad (5.42)$$

The ghost-line momentum in this case pairs with momentum p_2.

The difference of these two diagrams is actually given by the divergence of the four-gluon vertex as can be seen below:

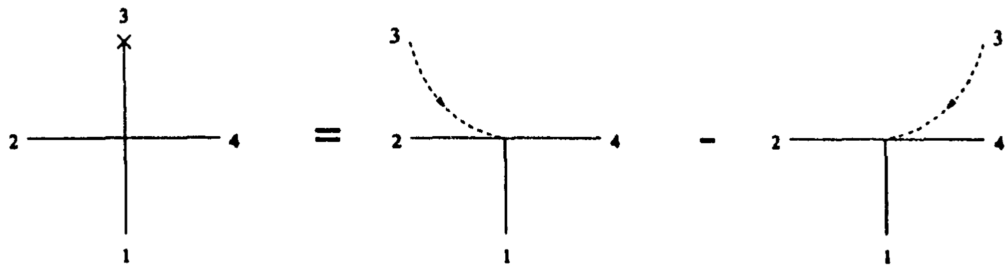

FIG. 22. An identity about a four-gluon vertex

This identity follows from rule 2, and the expression for the derivative of the four-gluon vertex

$$
\begin{aligned}
& ig^2(p_3)_3(-g_{23}g_{14} - g_{12}g_{34} + 2g_{24}g_{13}) \\
&= ig^2(-g_{14}(p_3)_2 - g_{12}(p_3)_4 + 2g_{24}(p_3)_1)
\end{aligned}
\tag{5.43}
$$

obtained from Fig. 13.

5. new quark vertices

We considered before an extra ghost line entering into a triple-gluon vertex. This ghost line injects some extra momentum into the vertex but otherwise does absolutely nothing. The same is true when an extra ghost line enters a quark-gluon vertex. Since this vertex is independent of the momenta, the following graphical identity is obviously true.

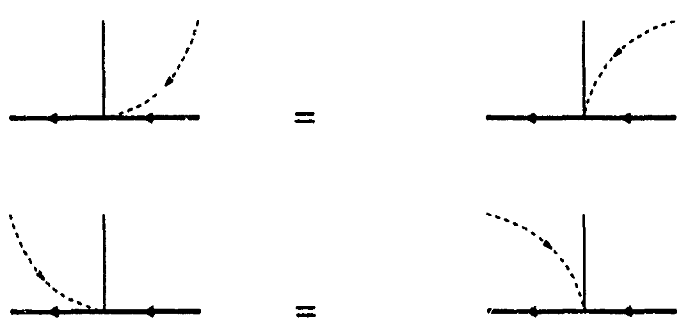

FIG. 23. New quark vertices

6. new four-gluon vertex

Again the ghost line entering into a four-gluon vertex does nothing but inject some momentum. However, the four-gluon vertex is momentum independent. Hence

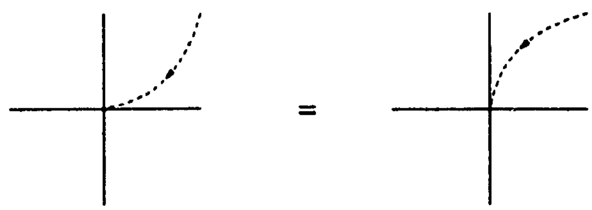

FIG. 24. New four-gluon vertices

7. external ends

If a diagram contains one of the following components, then the result of that diagram vanishes because of the absence of a pole to cancel the external on-shell Klein-Gordon or Dirac factors.

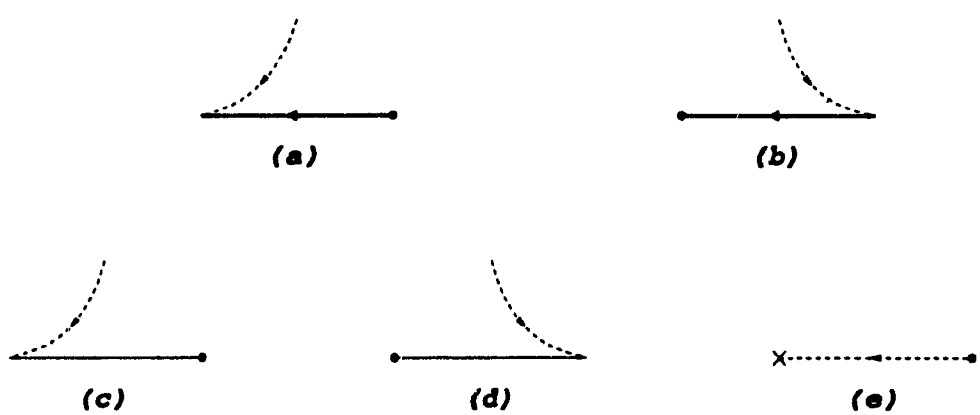

FIG. 25. External ends. The end of a line without dot *here* denotes an external end

Fig. 25(e) is true because this ghost line was originally a gluon line. As a result, a gluon wave function $\epsilon^{\mu}(k)$ is present, and the cross in the graph leads to a factor

$$k \cdot \epsilon(k) = 0 \ . \tag{5.44}$$

D. Gauge invariance of QCD scattering amplitudes

Using these rules, the gauge variation (*i.e.*, the divergence of a gluon line) of a Feynman diagram can be represented by a summation of several diagrams. For example, the diagram Fig. 27(i) can be changed into two diagrams as shown in Fig. 26.

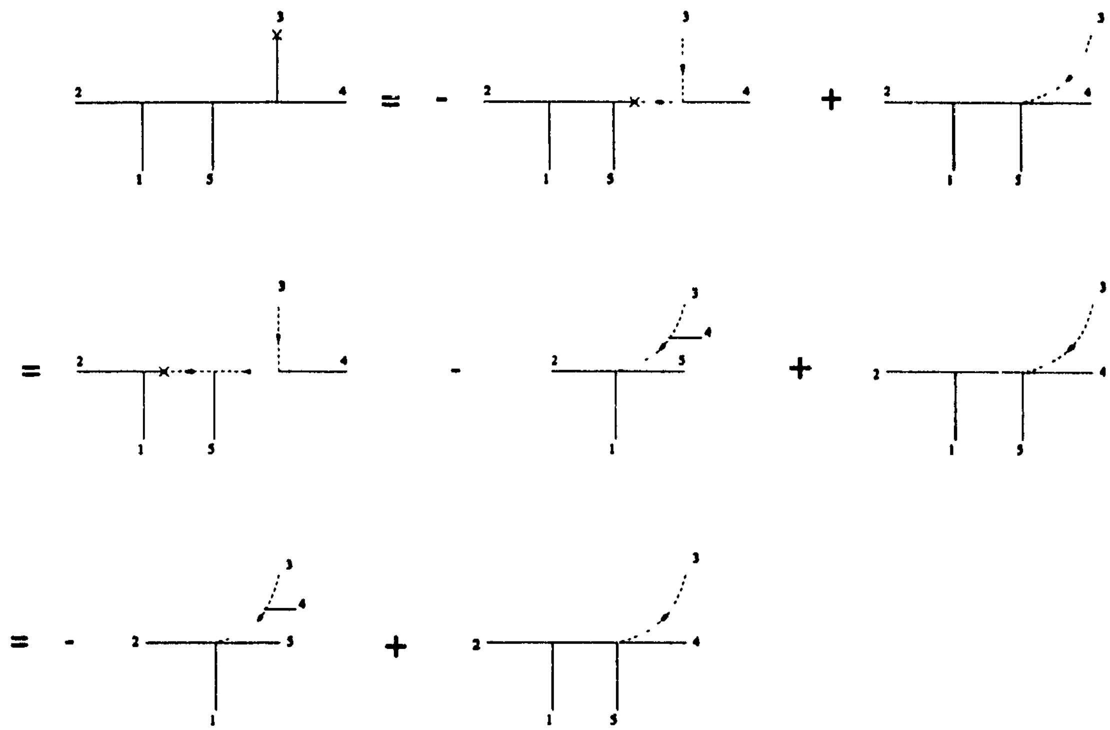

FIG. 26. An example about how to change the variation of a Feynman diagram into sum of several diagrams

A sum of a set of Feynman diagrams will be gauge invariant if and only if these diagrams obtained from the gauge variations manage to cancel one another. We will first illustrate how this is accomplished with a few explicit examples.

1. examples

Consider the sum of color-oriented diagrams in Fig. 27 , all with the same $U(N)$ (or $SU(N)$) color factors. Using the rules in the subsection above, their gauge variations are given by the sum of diagrams in Fig. 28. Diagrams that are trivially zero (such as those in Fig. 25) are omitted. These diagrams cancel one another and the result is zero at the end. Consequently the sum of the diagrams in Fig. 27 (without the cross) is gauge invariant.

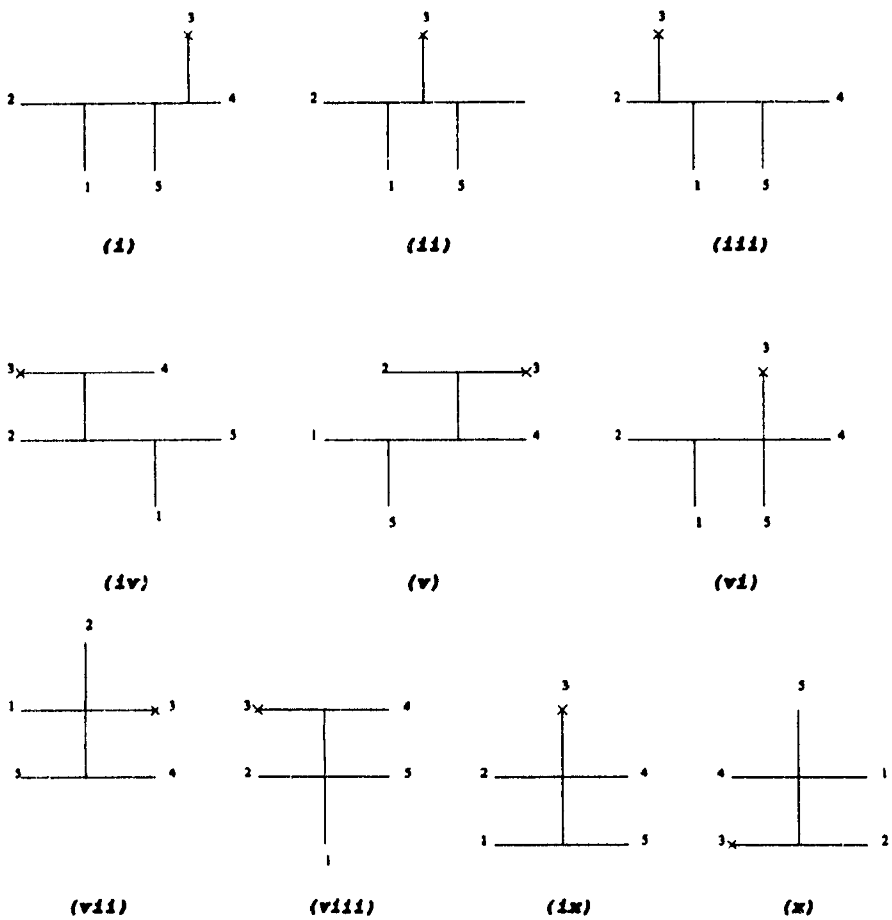

FIG. 27. All the Feynman diagrams of a five-point function at tree level which carry the given color factor.

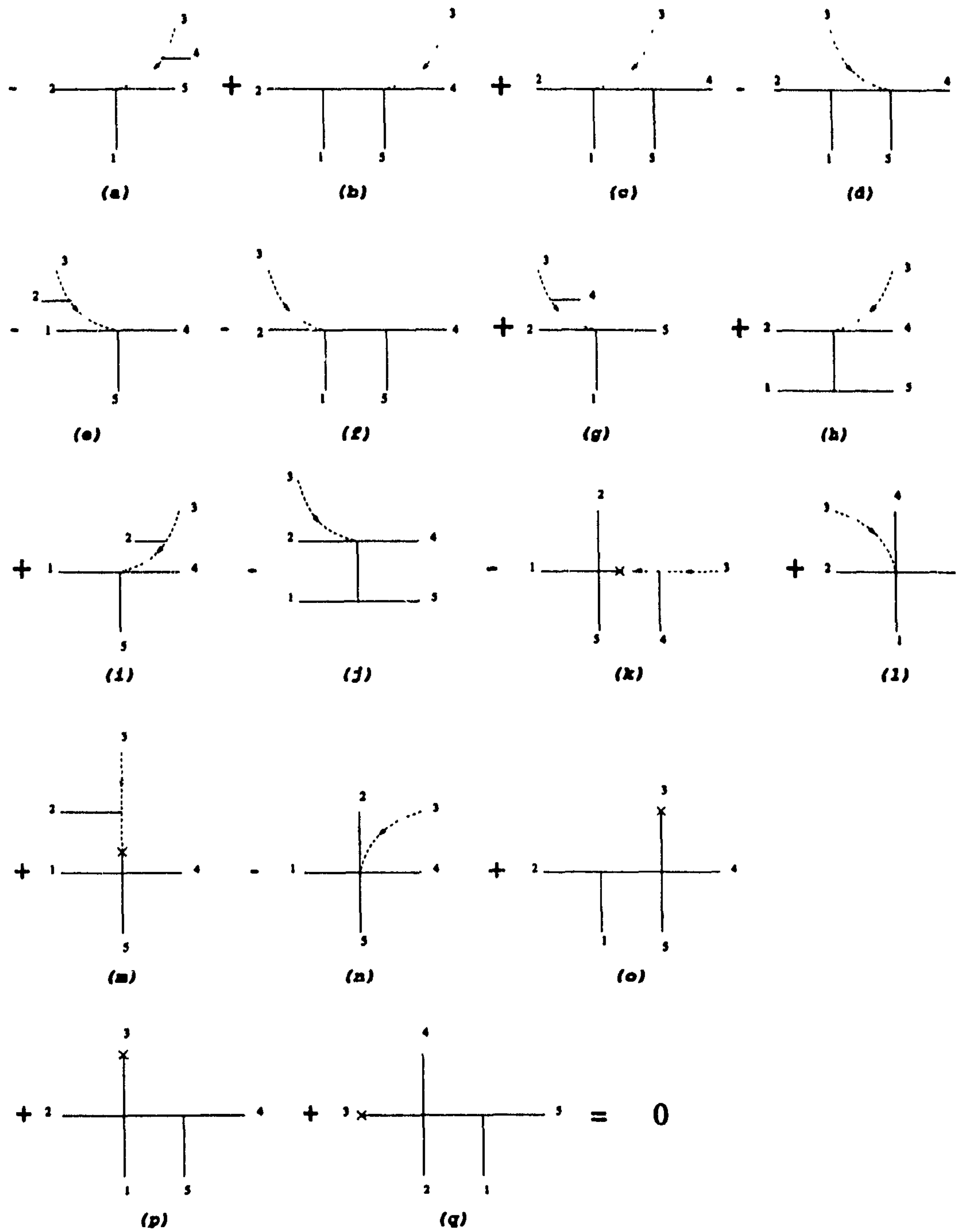

FIG. 28. Gauge invariance of the five-point amplitude at tree level. Explicitly, (a) and (b) are from (i) in the previous Fig; (c) and (d) are from (ii); (e) and (f) are from (iii); (h) and (g) are from (iv); (i) and (j) are from (v),(k) and (l) are from (viii); (m) and (n) are from (x). (o), (p) and (q) are just (vi), (vii), and (ix) respectively.

According to the rules we presented in previous subsection, we can see that the sums of the following diagrams in Fig. 28 are zero:

(i) a, g, k;

(ii) b, d, o;

(iii) c, f, p;

(iv) h, j, q;

(v) e, i, m;

(vi) l, n.

2. general arguments

Now we see how these rules work in general.

To start with, let us review the rules again. When a cross (divergence) is applied to the end of a gluon line, two types of diagrams may appear unless this gluon line is directly connected to a ghost-gluon vertex, or a four-gluon vertex. These are the sliding diagrams and the substitution diagrams (rules 1,2). The cross disappears in the sliding diagrams, but it travels forward in the substitution diagrams, allowing these rules to be applied again. Repeating this over and over, the surviving cross either ends up (i) at an external gluon line, (ii) on a four-gluon vertex, or (iii) on a ghost-gluon vertex. In case (i), the corresponding diagram disappears because of rule 7. The remaining diagrams of case (ii) and case (iii) as well as the diagrams without a cross must add up to zero for a gauge-invariant combination of diagrams. We shall discuss below how this can happen.

The sliding diagrams have the following characteristics: those that slide to the left have a minus sign, and those that slide to the right have a plus sign. Moreover, the ghost line that slides into a vertex does not alter the vertex except to inject into it an appropriate momentum Such injected momenta could affect only a triple-gluon vertex (rules 4,5,6) which is momentum-dependent. In principle it could also affect a ghost-gluon vertex when the sliding ghost is paired with the outgoing ghost of the vertex, but such a diagram never appears.

When a sliding ghost ends up at a quark-gluon vertex, it could have come from the left or from the right with the *same* color factor, but these two differ by a sign so their sum is zero as shown in Fig. 29.

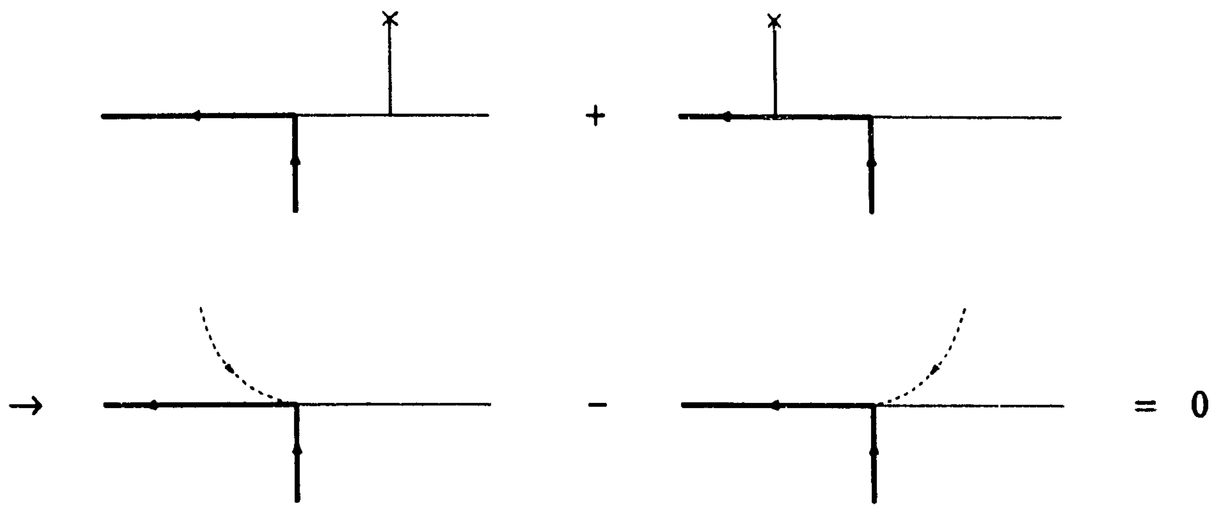

FIG. 29. Cancellation involved quark vertices.

Note that in this figure and all the figures below, the graphs shown are meant to be only a portion of a possibly much larger Feynman diagram. In other words, the lines shown in the graphs may very well be connected to other lines not explicitly drawn.

As shown in Fig. 30, a three-gluon vertex divides the plane around the vertex into three sectors, each bounded by a pair of gluons. A sliding ghost ending up at a three-gluon vertex is paired up with a gluon line in one of these three sectors. Depending on whether it pairs up with the left or the right gluon line in the sector, the sign differs. According to rule 4, these two add up to be zero together with the diagram obtained by replacing the sliding ghost line with a gluon line having a cross on top.

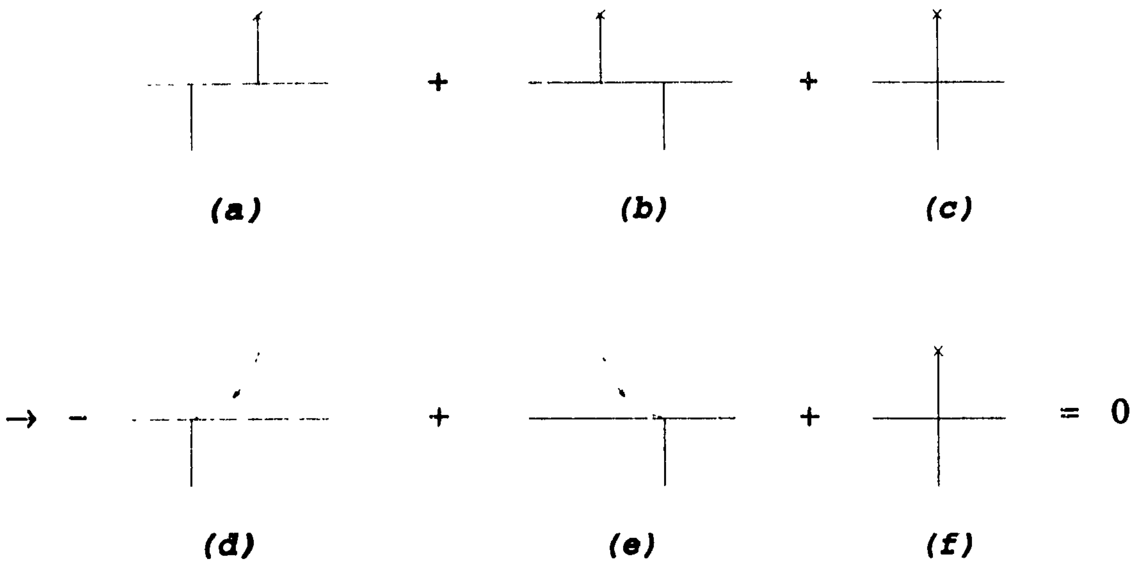

FIG. 30. Cancellation involved triple-gluon and four-gluon vertices.

Similarly, if a sliding ghost line ends at a four-gluon vertex, the left one and the other one have a relative sign different, and they cancel as shown in Fig. 31.

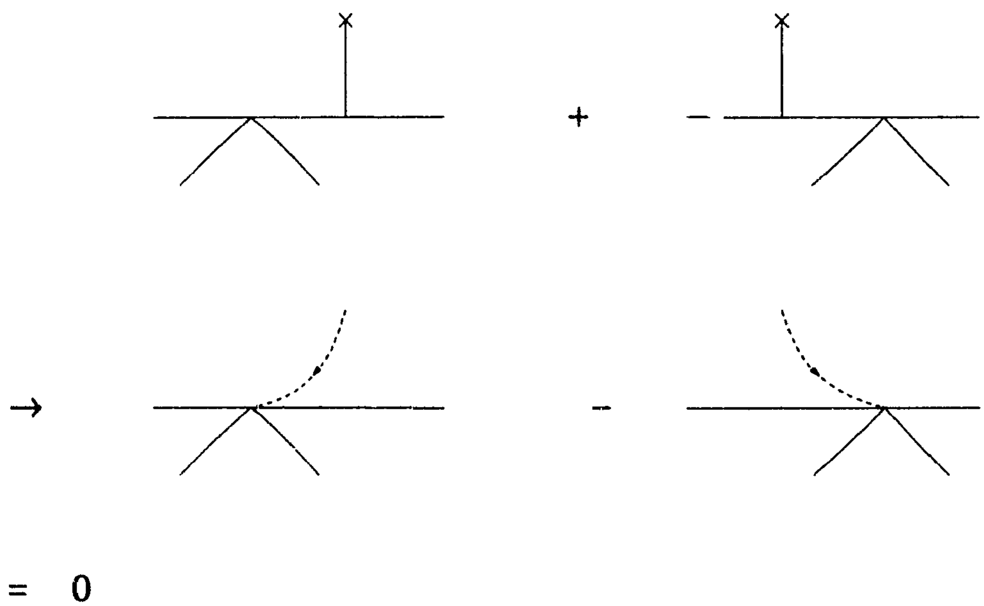

FIG. 31. Cancellation involved four-gluon vertices.

Finally, a sliding ghost can end up at a ghost-gluon vertex, paired with the gluon line, either (i) in the sector bounded by the gluon and the incoming ghost of the vertex, or (ii) the sector bounded by the gluon and the outgoing ghost of the vertex. In both of these cases, it is important to note that the ghost lines in the vertex must appear in the diagram in the form of a closed loop. The cancellation in both cases relies on the complementary diagram where the ghost loop is replaced by a gluon loop.

Let us first discuss (i). First notice that the sliding ghost line may be paired up with the incoming ghost line instead, because of the absence of momentum dependence of the vertex on these lines.

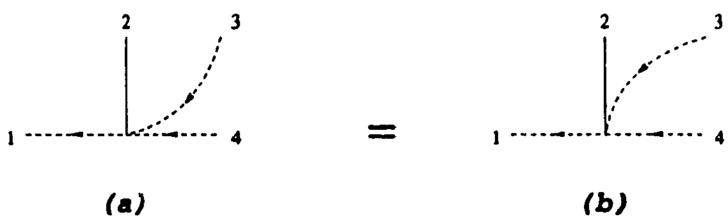

FIG. 32. A graphical identity about ghost vertex.

Secondly, the cancellation proceeds by rule 3 as follows.

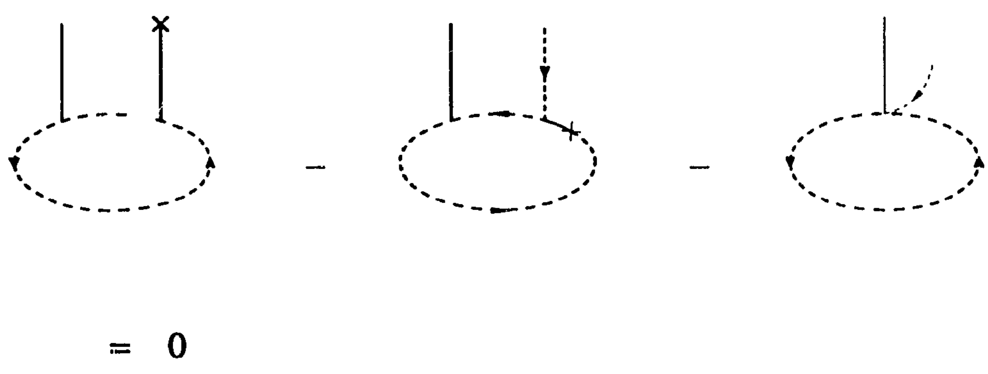

FIG. 33. One of the cancellations involved ghost vertices.

The remaining question is where the diagrams in Fig. 33 can come from. The answer of this is shown below.

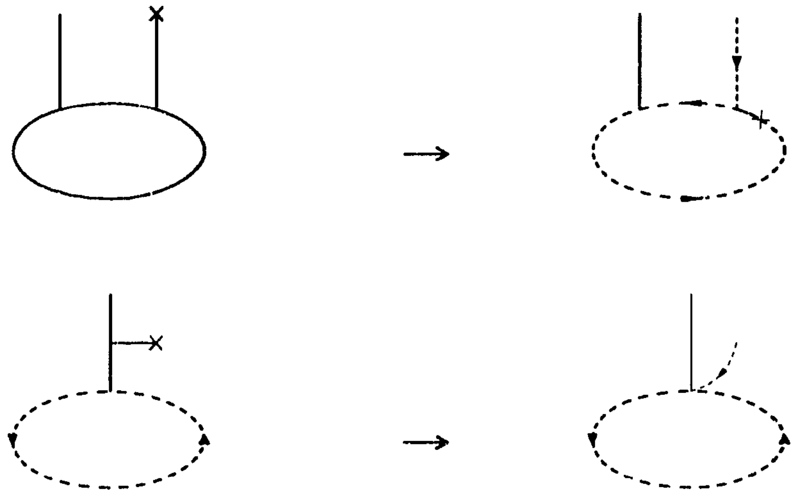

FIG. 34. The original diagrams of those in the previous Figure.

This concludes the discussion of (i). The cancellation involving case (ii) is shown below.

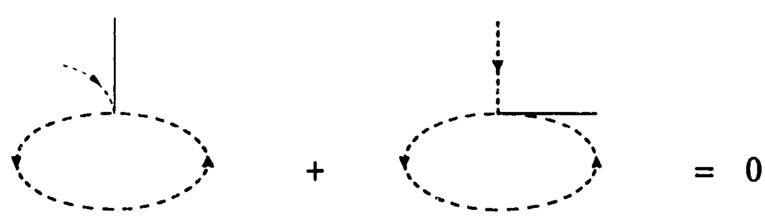

FIG. 35. The other cancellation involved ghost vertices.

And all the diagrams in Fig. 35 can be obtained as shown in Fig. 36.

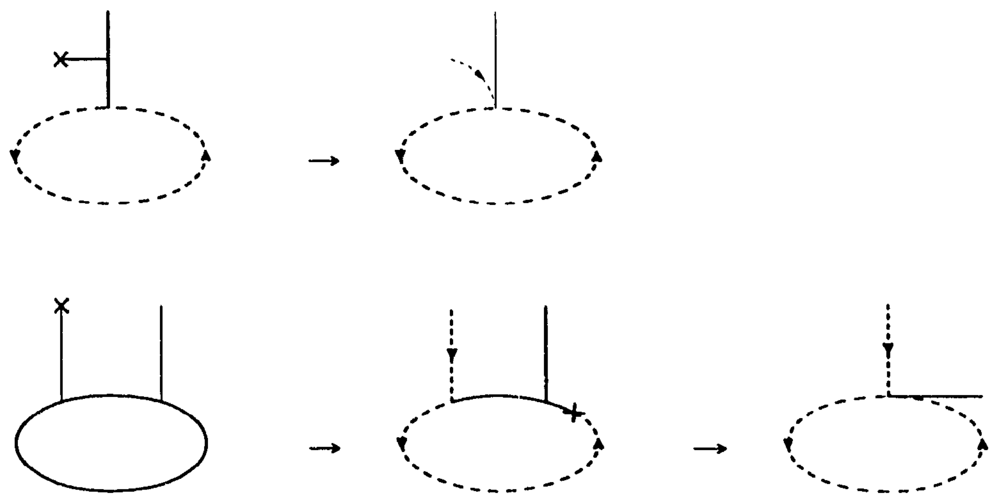

FIG. 36. The original diagrams of those in Fig. .

In summary, the sum of all color-oriented diagrams for a fixed color factor and *with a fixed number of quark loops* is invariant under gauge transformation of any of its external gluon wave functions.

VI. CONCLUSION

In conclusion, a set of graphical rules inspired by BRST invariance has been derived and applied to prove the explicit gauge invariance of QED and QCD, especially perturbative ones at multi-loop level. These rules show us how the gauge variation of each individual Feynman diagram or color-oriented diagram cancel each other when we sum up all the contributions to a gauge invariant subset of them.

Compared with the original Feynman rules shown in Appendix B, we find that these new graphical rules make explicit use of the property of the divergence (indicated by a × in the diagrams). These rules separate out the longitudinal component of an external gluon and introduce 'new' vertices to describe the traveling and the coupling of this component. On the other hand, in the original Feynman rules, the longitudinal component is mixed up with other components, and gauge invariance is thus obscured.

It is conceivable that even smaller gauge-invariant subsets can be obtained in specific gauges like the background gauge [16]. This problem is under investigation. Another direction for study is related to the so-called string-reorganization, one of its aims being an attempt to sum up the individual gauge-dependent Feynman diagrams into a single gauge-independent 'dual' expression. This has been achieved in QED [17] but not yet in QCD, and it is hoped that the additional insights gained from the present work could help to attain this goal. This is an important objective [18] because it may help to simplify practical computations. As mentioned in the Introduction, the number of Feynman diagrams involved in a higher-point or a multi-loop amplitude is very large. For example, a tree-level six-point pure-gluon amplitude already has hundreds of Feynman diagrams [19], and the practical calculation for this amplitude is thus extremely lengthy. An important part of this complexity arises because individual Feynman diagrams are gauge dependent, so in evaluating them individually many gauge-dependent terms have to be carried along, which eventually mus be cancelled out in the sum to obtain the physical amplitude. If a single 'dual' expression can be developed for the sum, which then must be gauge invariant, such additional labour of dealing with the gauge-dependent terms can hopefully be saved.

ACKNOWLEDGMENTS

I want to thank my supervisor Professor C.S.Lam. I am grateful to his suggestion to this subject, and his great patience to answer all my various questions. Prof. Lam helped me to correct many mistakes in the first scripts. Also I take this chance to thank my comrade S.Vatche for a lot useful discussions. Especially I want to thank Ms T. Rhama for helping me to translate the abstract into French. This research is partially supported by Dow Hickson fellowship.

APPENDIX A: THE CHAN-PATON FACTORS FOR MULTI-LOOP ARBITRARY PROCESSES

In this Appendix we are going to prove the statement in Sec III, that the generalized Chan-Paton color factors for $U(N)$ are mutually orthogonal in the large N limit. As we shall discuss later, the Chan-Paton factor is made up of products of $U(N)$ generators T^a in the fundamental representation and their traces. Before going into the details, it would be useful first to develop a convenient set of mathematical notations.

Fig. 37(a) represents the trace of a product of generators. Specifically, each dot on the line represents a generator matrix T^x, and the solid lines between dots represent indices of the matrix elements. If two dots are joined by a line, then they represent two matrices sharing a common index, which is to be summed over. We choose a convention to read these matrices in the opposed direction of the arrow on a line. Therefore, the *ring* in Fig. 37(a) means $tr(T^aT^bT^cT^dT^e)$, the line in Fig. 37(b) represents $(T^aT^bT^cT^dT^e)_{ij}$.

Consider each Chan-Paton factor as a vector, whose components are labelled by the color indices of the generators in that factor. Inner products can be defined between some of these vectors. An example in shown in Fig. 37(c), which represents the inner product $A \cdot \tilde{A}$, defined to be

$$A \cdot \tilde{A} = \frac{1}{K} \sum_{a,b,c,d,e} (tr(T^aT^bT^cT^dT^e)tr(T^eT^dT^cT^bT^a)) \,, \tag{A1}$$

where K is the normalization constant, and

$$\begin{aligned} A &= tr(T^aT^bT^cT^dT^e) \,, \\ \tilde{A} &= tr(T^eT^dT^cT^bT^a) \,. \end{aligned} \tag{A2}$$

Note the lower *ring* in Fig. represents the dual vector of A, instead of A itself. Similarly, the inner product shown in Fig. (d) represents

$$A \cdot \tilde{B} = \frac{1}{K} \sum_{a,b,c,d,e} tr(T^aT^bT^cT^dT^e)tr(T^bT^aT^d)tr(T^eT^c) \,, \tag{A3}$$

$$A = tr(T^aT^bT^cT^dT^e) \,, \quad B = tr(T^dT^aT^b)tr(T^eT^c) \,. \tag{A4}$$

We can calculate these two examples explicitly to find out the normalization factor K for these dot products. First Fig. 37(c),

$$
\begin{aligned}
A \cdot \tilde{A} &= \frac{1}{K} \sum_{a,b,c,d,e} (tr(T^a T^b T^c T^d T^e) tr(T^e T^d T^c T^b T^a)) \ , \\
&= \frac{1}{K} \sum_{a,b,c,d,e} (T^a)_{ij} (T^b)_{jk} (T^c)_{kl} (T^d)_{lm} (T^e)_{mi} (T^e)_{i'j'} (T^d)_{j'k'} (T^c)_{k'l'} (T^b)_{l'm'} (T^a)_{m'i'} \ , \\
&= \frac{1}{K} (\delta_{ii'} \delta_{jm'} \delta_{jm'} \delta_{kl'} \delta_{kl'} \delta_{lk'} \delta_{lk'} \delta_{mj'} \delta_{mj'} \delta_{ii'}) \ , \\
&= \frac{1}{K} (N^5) \ . \qquad \text{(A5)}
\end{aligned}
$$

Then Fig. 37(d),

$$
\begin{aligned}
A \cdot \tilde{B} &= \frac{1}{K} \sum_{a,b,c,d,e} tr(T^a T^b T^c T^d T^e) tr(T^d T^a T^b) tr(T^e T^c) \ , \\
&= \frac{1}{K} \sum_{a,b,c,d,e} (T^a)_{ij} (T^b)_{jk} (T^c)_{kl} (T^d)_{lm} (T^e)_{mi} (T^e)_{i'j'} (T^c)_{j'i'} (T^d)_{k'l'} (T^a)_{l'm'} (T^b)_{m'k'} \ , \\
&= \frac{1}{K} \sum_{a,b,c,d,e} (\delta_{im'} \delta_{jl'} \delta_{jk'} \delta_{km'} \delta_{ki'} \delta_{lj'} \delta_{ll'} \delta_{mk'} \delta_{mj'} \delta_{ii'}) \ , \\
&= \frac{1}{K} \sum_{a,b,c,d,e} (\delta_{jj} \delta_{ii}) \ , \\
&= \frac{1}{K} (N^2) \ . \qquad \text{(A6)}
\end{aligned}
$$

Note that this is much smaller than $A \cdot \tilde{A}$ in the large-N limit.

A general rule for the inner products can be worked out. The result is the following. Cover the inner-product graphs by a *complete set* of closed *paths.* The final result is N^n/K, where n is the number of such closed paths. A closed path is drawn starting from any point at a solid line, proceeding along the arrow until it comes to a dot, whence it must follow the dash line to cross over to the other solid line. Continue thus until the path returns to the starting point to form a closed path. A complete set of closed paths is obtained when every solid line is covered once by a path and every dash line is covered twice by some paths.

Using this rule, we can proceed to prove the claim of Sec. III, first for gluon amplitudes, whose Chan-Paton factor is a product of traces

$$
c = \prod tr(T^{a_1} \cdots T^{a_j}) \qquad \text{(A7)}
$$

in which each external color index appears once. Now we can prove the following two statements.

1. In the vector space with n color indices, the normalization factor $K(n)$ is N^n. If the color factor c consists of only one trace,

$$c = tr(T^{a_1}T^{a_2}\cdots T^{a_n}) \equiv A \ , \tag{A8}$$

then this follows immediately from the rule because

$$A \cdot \tilde{A} = \frac{1}{K(n)} \sum_{a_1,a_2\cdots a_n=1}^{N} tr(T^{a_1}T^{a_2}\cdots T^{a_n})tr(T^{a_n}T^{a_{n-1}}\cdots T^{a_1}) = \frac{N^n}{K(n)} = 1 \ . \tag{A9}$$

For a more general case, consider

$$c = \prod_j tr(\prod{}' T^i) \equiv \prod_j A_j \ , \tag{A10}$$

where $\prod'$ means non-commutative product. Then the inner product becomes

$$\begin{aligned} c \cdot \tilde{c} &= \prod_j A_j \cdot \tilde{A}_j \ , \\ &= \frac{1}{K(n)} \prod_j N^{n_j} = \frac{N^n}{K(n)} = 1 \ , \end{aligned} \tag{A11}$$

where n_j is the number of closed paths in A_j. Hence the claim is once again valid.

2. One and zero are the only possible results for these inner products if N trends to infinity. To prove that, consider the inner product of two vectors A and B and its corresponding graph. There are $2n$ pieces of solid lines connecting the dots. Since each closed path must contain at least two pieces of such solid lines, and since each solid line can be passed only once, we can conclude that the maximum number of these closed graphs is n, and the statement above becomes obvious considering the infinite limit of N.

Now we are going to prove the statement made in Sec III: the inner product of two n-vectors A and B is one if $A = B$ up to cyclic permutation. Otherwise the inner product is zero.

At tree level, where A and B each contains only one trace, the proof is quite obvious. If $A = B$ up to cyclic order, then for any two adjacent points a, b in the upper *ring*, the corresponding two points a, b in the lower *ring* will also be adjacent, but in the opposite order. Therefore, each closed path we construct will contain exactly two pieces of solid lines, and we can obtain the maximum number of closed paths. As a result, the inner product is 1.

If $A \neq B$, then there must be at least one pair of adjacent dots a, b in the upper *ring* for which the corresponding dots in the lower *ring* are either not adjacent, or adjacent but in the same order. For both cases, the closed path involving points a, b will contain more than two pieces of solid lines. This reduces the total number of closed paths we get, and the inner product is thus zero.

For multi-loop cases, as we can see from the examples in Sec. III, the Chan-Paton factor is in general a product of traces as defined in (A7). If $A = B$, then all the traces in A must pair up with those traces in B. For each pair of traces we can use the above argument, and the inner product we get is one. If $A \neq B$, then there is at least one trace in A that is not the same as its partner in B. We will get less number of closed paths, so that the inner product of these two vectors is zero.

We have so far ignored external quarks. Their inclusion is not at all difficult. The Chan-Paton factor for each quark line is either the identity matrix, or a product of generators. The Chan-Paton factor for the whole diagram consists of the product of the quark factors, and some traces. For a quark factor like

$$B = (T^{a_1}T^{a_2}\cdots T^{a_m})_{kl} \ , \tag{A12}$$

where kl are the color indices of the external quarks and m is the number of the external gluons attached to this quark line, the inner product of two such factors is defined to be

$$B \cdot \tilde{B} = \frac{1}{N^{m+1}} \sum_{a_i} ((T^{a_1}T^{a_2}\cdots T^{a_m})_{kl}((T^{a_m}\cdots T^{a_2}T^{a_1})_{lk} = 1 \ . \tag{A13}$$

which can be read off from Fig. 37(e) .

Consider a scattering diagram involving $2n$ external quarks and m external gluons. The Chan-Paton factors that span the vector space consist of a products of factors of the form (A12), together with a product of trace factors of the form (A2) and (A4). The inner product of two such factors with a fixed n and m will again be defined to be the product of one with the dual of another, summed over all gluon and quark color indices, and divided by N^{n+m}. By exactly the same kind of argument as before, the inner product between two such factors A and C can be represented graphically, *e.g.*, Fig. 38. Their dot product would be zero unless $A = C$, for otherwise the number of closed paths would be less than the maximum number possible. This then completes the proof of our claim.

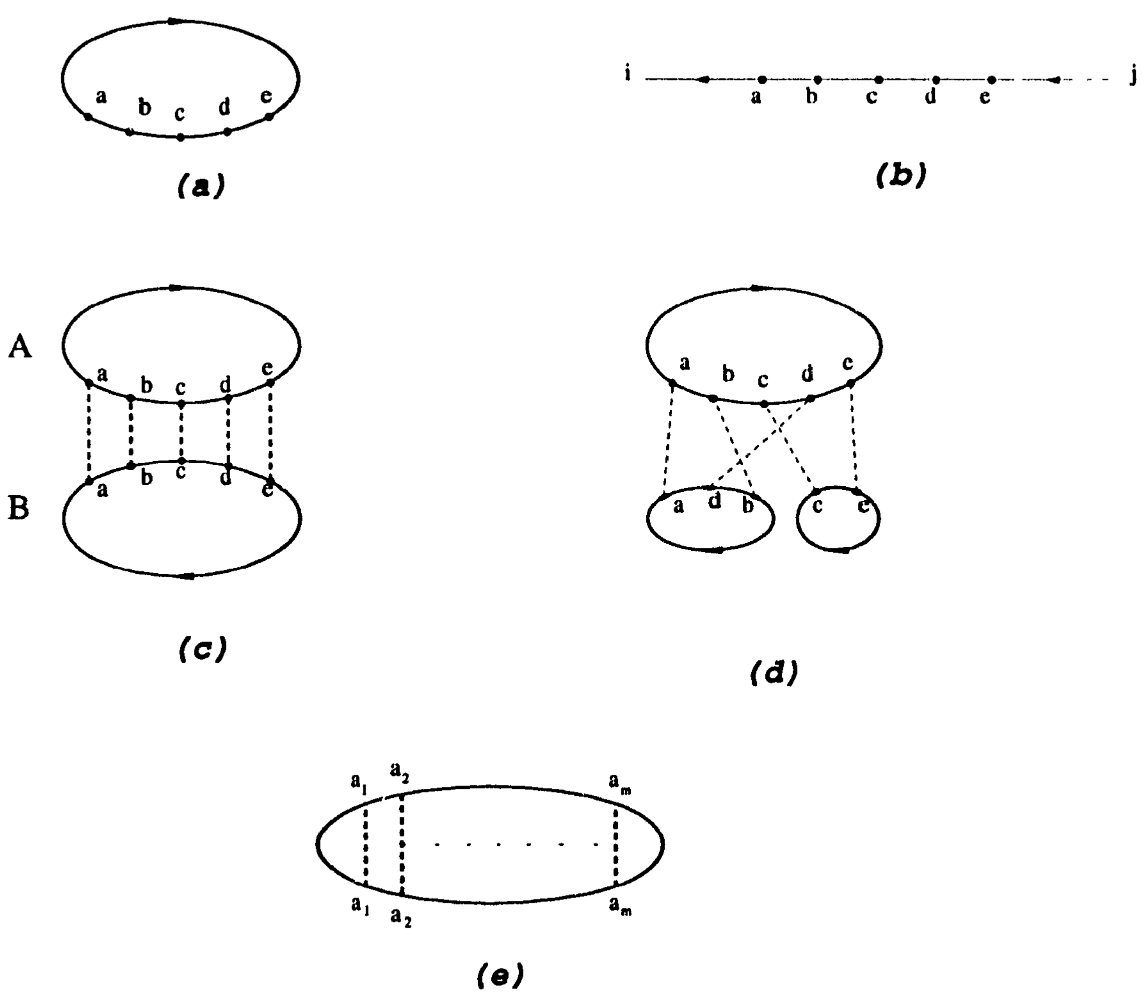

FIG. 37. Color graphs

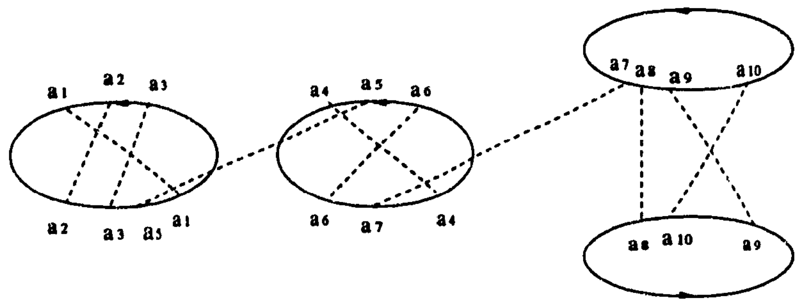

FIG. 38. An example of inner product of two color factors. For simplicity, we omit the dots at the joining points of a dash line and a solid line here.

APPENDIX B: FEYNMAN RULES FOR QED AND QCD

The Lagrangian for QED is

$$L= \bar{\psi}((i\gamma_\mu D^\mu) - m)\psi - \frac{1}{4}F^{\mu\nu}F_{\mu\nu} - \frac{1}{2\lambda}(\partial \cdot A)^2 \,, \tag{B1}$$

From the *free* Lagrangian, the quadratic terms, for ψ

$$L_f = \bar{\psi}i(\partial_\mu\gamma^\mu - m)\psi \,, \tag{B2}$$

we can get the two-point Green function, or say propagator, as

$$\begin{aligned} i\Delta_f(p)&= \frac{i}{p_\mu\gamma^\mu - m + i\epsilon} \\ &= \frac{i(p_\mu\gamma^\mu + m)}{p^2 - m^2 + i\epsilon} \,. \end{aligned} \tag{B3}$$

It can be denoted graphically as Fig. 39(a).

For an internal photon line, the free Lagrangian including the gauge fixing term

$$-\frac{1}{2\lambda}(\partial \cdot A)^2 - \frac{1}{4}(F_{\mu\nu}F^{\mu\nu}) \,, \tag{B4}$$

and we have the propagator as

$$i\Delta_{ph}(p)_{\mu\nu} = \frac{-ig_{\mu\nu} + (1-\lambda)p^\mu p^\nu / p^2}{p^2 + i\epsilon} \,. \tag{B5}$$

The most common choice is Feynman gauge $\lambda = 1$. This propagator can be shown as Fig. 39(b).

The interaction term between fermion and the photon is

$$ie\gamma_\mu \bar{\psi} A^\mu \psi \,, \tag{B6}$$

so that the vertex factor is

$$-ie\gamma_\mu \tag{B7}$$

It is shown in Fig. 39(c).

Incoming and outgoing electrons are represented as $u(p)$ and $\bar{u}(p)$ respectively.For incoming and outging positrons, write $v(p)$ and $\bar{v}(p)$. For external photon line, multiply the polarization vector $\epsilon_\mu(p)$.

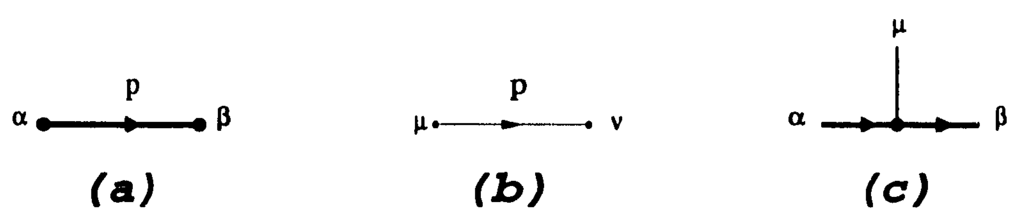

FIG. 39. QED Feynman rules, with the bold line for fermion line, the thinner solid line for photon

Therefore for each scattering amplitude,

1) We use the Fig. 39(a), (b), and (c) as basic elements and construct all possible diagrams, the Feynman diagrams. Then for each fermion, photon internal line and vertex, write down the corresponding factors as given above. Multiply these factors together.

2)Insert an additional (-1) for each close fermion loop.

3)Integrate over all the internal loop momenta using

$$\int \frac{d^4q}{(2\pi)^4} \tag{B8}$$

4)Fermion loop should occur twice, clockwise and anti-clockwise directions

5)Multiple the relative minus sign due to exchanging the equivalent external fermion lines, and also the symmetry factor.

Then sum up the contributions from all the diagrams, we get the scattering amplitude.

As for QCD, the effective Lagrangian we got in Sec II is much more complex than the QED one.

$$L_{eff} = \bar{\Psi} i(D_\mu \gamma \mu - m)\Psi - \frac{1}{4}(F^a_{\mu\nu})^2 - \frac{1}{2\lambda}(\partial \cdot A)^2 - \bar{c}^a \partial^\mu D_\mu c^a \ . \tag{B9}$$

Using the same method as that for QED, we can write the propagators for all the particles.

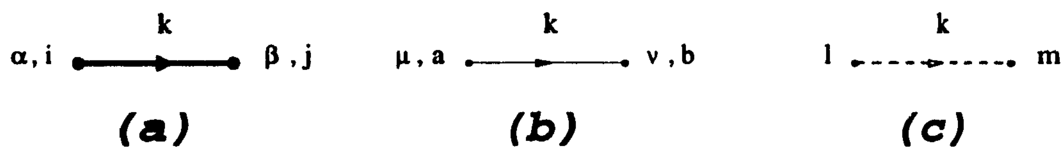

FIG. 40. QCD Feynman rules, with the bold line for quark line, the thinner solid line for gluon, and dash line for ghost.

1)gluon propagator

$$iD_F^{ab}(k)_{\mu\nu} = \frac{-i\delta^{ab}}{k^2 + i\epsilon}\left[g_{\mu\nu} + (\lambda - 1)k_\mu k_\nu / k^2\right] \ , \tag{B10}$$

as in Fig. 40(a)

2)quark progator

$$iS_F^{ij}(p)_{\alpha\beta} = \left(\frac{i\delta^{ij}}{p_\mu \gamma^\mu - m + i\epsilon}\right)_{\alpha\beta} \ , \tag{B11}$$

as in Fig. 40(b).

3)ghost propagator is

$$i\Delta_F^{lm} = \frac{i\delta^{lm}}{k^2 - m^2 + i\epsilon}\,, \tag{B12}$$

as shown in Fig. 40(c).

In QCD there are more vertices:

1)triple-gluon vertex

$$i\Gamma^{abc}_{\mu\nu\lambda} = igf^{abc}((k_1 - k_2)_\lambda g_{\mu\nu} + (k_2 - k_3)_\mu g_{\nu\lambda} + (k_3 - k_1)_\nu g_{\mu\lambda})\ . \tag{B13}$$

2)four-gluon vertex

$$\begin{aligned} i\Gamma^{abcd}_{\mu\nu\lambda\rho} = -ig^2(&f^{abe}f^{cde}(g_{\mu\lambda}g_{\nu\rho} - g_{\nu\lambda}g_{\mu\lambda}) \\ &+ f^{ace}f^{bde}(g_{\mu\nu}g_{\rho\lambda} - g_{\nu\lambda}g_{\mu\rho}) \\ &+ f^{ade}f^{cbe}(g_{\mu\lambda}g_{\rho\nu} - g_{\rho\lambda}g_{\mu\nu}))\ . \end{aligned} \tag{B14}$$

3)gluon-ghost vertex

$$i\Gamma^{abc}_\mu = gf^{abc}k_\mu\ . \tag{B15}$$

4)gluon-quark vertex

$$i\Gamma^{abc}_\mu = gf^{abc}k_\mu\ , \tag{B16}$$

All these vertices are show in Fig. 41 (a), (b), (c) and (d) respectively.

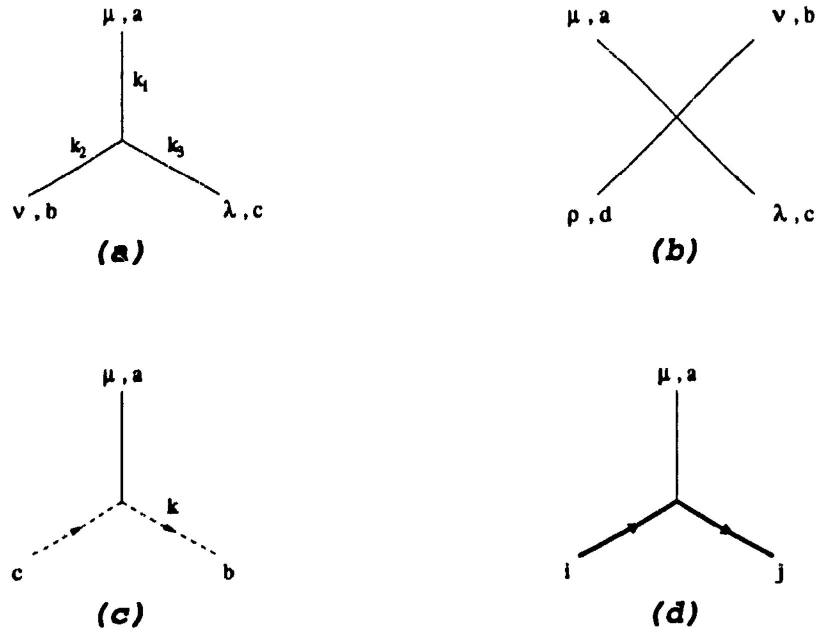

FIG. 41. QCD Feynman rules, with the bold line for quark line, the thinner solid line for gluon, and dash line for ghost.

Then we can calculate the scattering amplitude as in QED.

REFERENCES

[1] C. N. Yang, R. Mills, Phys. Rev. **96** (1954), 191.

[2] Z. Xu, D. H. Zhang, and L. Chang, Tsinghua University Preprints, Beijing, China, TUTP-84/4, TUTP-84/5, TUTP-84/6, Nucl.Phys. **B291** (1987), 392.

[3] P. De Causmeaker, R. Gastmans, W. Troost and T. T. Wu, Phys. Lett. **105B** (1981), 215; Nucl.Phys. **B206** (1982), 53.

F. A. Berends, R. Kleiss, P. De Causmeaker, R. Gastmans and T. T. Wu, Nucl. Phys. **B206** (1982), 61.

[4] C. S. Lam, Nucl. Phys. **B397** (1993) 143; Phys. Rev. **D48** (1993), 873.

[5] C. S. Lam and J. P. Lebrun, Nuovo Cimento **59A** (1969), 379.

[6] Ta-Pei Cheng, Ling-Fong Li, Gauge Theiry of Elementary Particle Physics, Oxford University press, 1984.

[7] G. Sterman, Quantum Field Theory, Cambridge University, 1993.

[8] J.C. Ward, Phys. Rev. **78** (1950). 182.

Y. Takahashi, Nuovo Cim. **6** (1957), 371.

[9] C. Becchi, A. Rouet, and R. Stora, Commun. Math. Phys. **42** (1975), 127.

[10] J. C. Taylor, Nucl. Phys. **B33** (1971), 436;

A. A. Slavnov, Teor. Mat. Fiz. **10** (1972), 153.

[11] J. Paton and Chan Hong-Mo, Nucl.Phys. **B229** (1983), 372.

[12] M. Managano, S. Parke and Z. Xu, Nucl. Phys. **B298** (1988), 653.

[13] F. A. Berends and W. Giele, Nucl. Phys. **B294** (1987), 700.

[14] Z. Bern and D. K. Koswor, Nucl. Phys. **B379** (1992), 451.

[15] G. t' Hooft, Nucl. Phys. **B72** (1974), 461.

[16] L. F. Abott, Nucl.Phys. **B185** (1981), 189;

L. F. Abott, M. T. Grisaru and R. K. Schaefer, Nucl. Phys. **B229** (1983), 372.

[17] Y. J. Feng and C. S. Lam, preprint, McGill/94-21, to be published.

[18] F. Wilczek, talk given at Cornell Lepton-Photon conference, hep-ph 9311302.

[19] M. L. Mangano, S. J. Parke, Fermilab-Pub-90/113-T(1990).